CR-172005

FINITE ELEMENT TECHNIQUES FOR THE NAVIER-STOKES EQUATIONS IN THE PRIMITIVE VARIABLE FORMULATION AND THE VORTICITY STREAM-FUNCTION FORMULATION.

by

F. Glaisner [1]

and

T.E. Tezduyar [2]

Department of Mechanical Engineering
University of Houston
Houston, TX 77004

Interim Report for the
Work Performed Under NASA-Johnson Space Center
Contract NAS 9-17380

July 1987

(1) Graduate Research Assistant
(2) Assistant Professor

ABSTRACT

Finite-element procedures for the Navier-Stokes equations in the primitive variable formulation and the vorticity stream-function formulation have been implemented.

For both formulations, streamline-upwind/Petrov-Galerkin techniques are used for the discretization of the transport equations.

The main problem associated with the vorticity stream-function formulation is the lack of boundary conditions for vorticity at solid surfaces. Here an implicit treatment of the vorticity at no-slip boundaries is incorporated in a predictor-multicorrector time integration scheme.

For the primitive variable formulation, mixed finite-element approximations are used. A nine-node element and a four-node + bubble element have been implemented. The latter is shown to exhibit a checkerboard pressure mode and a numerical treatment for this spurious pressure mode is proposed.

The two methods are compared from the points of view of simulating internal and external flows and the possibilities of extensions to three dimensions.

TABLE OF CONTENTS

CHAPTER 1: INTRODUCTION

Computational Fluid Dynamics (CFD) is one of the most challenging fields of applied sciences. It deals with all the aspects of flow engineering, from high speed reacting flows around a space vehicle entering the earth's atmosphere to flows in porous media encountered in resevoir engineering.

The common denominator of this wide range of problems is that their governing equations are usually three dimensional, time dependent and nonlinear. Moreover, the numerical treatment of practical problems involves the solution of very large systems of equations. In recent years, the development of supercomputers combining large in-core storage with very high computing speeds made it possible to deal with such problems. Given such hardware capability, the engineer's work is the development of numerical procedures adapted to the solution of specific classes of problems.

The present work is a contribution to the development of numerical schemes for the solution of the Navier-Stokes equations.

The use of the vorticity stream-function form of the Navier-Stokes equations is appropriate for the study of two-dimensional flows [1,2]. For two-dimensional situations, the vorticity stream-function equations reduce to a set of scalar equations so that the number of degrees of freedom of the problem is only two. Another main interest of that formulation is that the incompressibility constraint is automatically satisfied by the computed flow field. However, solving the vorticity transport equation presents difficulties due to the lack of boundary conditions at solid surfaces. A feature of this study is the proper numerical treatment of the boundary conditions for the vorticity at solid surfaces. A mixed finite-element formulation is used that allows the implicit computation of the trace of the vorticity on no-slip boundaries at each time step.

The primitive variable formulation of the Navier-Stokes equations is suited for two-dimensional and three-dimensional calculations, and the treatment of the boundary conditions presents no difficulties [3,4]. The major problem associated to that formulation is the necessity of using different orders of interpolation for the velocity and the pressure [5,6]. In the present study mixed finite-element interpolations using quadratic approximation for the velocity and linear approximation for the pressure have been used. A four-node + bubble element, and the nine-node Lagrange element have been tested.

A common problem associated to both formulations is the treatment of the advection term . It is well known that the Galerkin approximations, which lead to centered discretization of the convection term, may create numerical oscillations for convection-dominated problems especially in the presence of sharp gradients in the solution [7]. On the other hand, such schemes introduce no numerical dissipation. The schemes introducing streamline diffusion via a suitable Petrov-Galerkin formulation are more robust than the centered schemes; they behave nicely at sharp fronts but of course involve relatively more numerical dissipation especially for high wave numbers. Such procedures have been applied to various fluid dy-

namics and convection-diffusion-reaction problems [8-12]. In the present study, we employ streamline-upwind/Petrov-Galerkin (SUPG) formulations for the solution of the vorticity transport equation in the vorticity stream-function formulation and for the solution of the momentum equation in the primitive variable formulation. The weighting functions are based on temporal as well as spatial discretizations [11].

The present study has been devoted to the development of software for two-dimensional simulations. However, in the case of the primitive variable formulation, the selection of procedures and the design of the code are such that the extension to three dimensions would present no major difficulties. In the case of the vorticity stream-function formulation, the simplicity of the equations is related to the dimensionality of the problem and no extension to three dimensions is foreseen.

CHAPTER 2: PROBLEM STATEMENT

2.1 The velocity-pressure formulation

Let Ω be a domain of R^2 and T be a positive real number. The flow of a viscous incompressible fluid in $\Omega \times [0,T]$ is described by the Navier-Stokes equations: Momentum equation

$$\frac{\partial \mathbf{u}}{\partial t} + (\mathbf{u}.\nabla)\mathbf{u} = \nabla.\sigma \quad \text{in} \quad \Omega \times [0,T] \tag{2.1}$$

Continuity equation (Incompressibility constraint)

$$\nabla.\mathbf{u} = 0 \quad \text{on} \quad \Omega \tag{2.2}$$

where $\mathbf{u}(\mathbf{x},t) = \{u_i(\mathbf{x},t)\}_{i=1}^2$ is the velocity field, $\sigma(\mathbf{x},t) = \{\sigma_{ij}(\mathbf{x},t)\}_{i,j=1}^2$ is the Cauchy stress tensor. For simplicity, we assume that the density of external forces is zero. For a Newtonian fluid of unit density, the stress tensor is given as

$$\sigma = -p\mathbf{I} + 2\nu\epsilon(\mathbf{u}), \tag{2.3}$$

where p is the pressure and $\epsilon(\mathbf{u})$ is the tensor of rates of deformation, i.e,

$$\epsilon(\mathbf{u}) = \frac{1}{2}(\nabla\mathbf{u} + (\nabla\mathbf{u})^T) \tag{2.4}$$

We assume that the boundary Γ of Ω is sufficiently smooth and admits the following decomposition :

$$\Gamma = \overline{\Gamma_g \cup \Gamma_h} \tag{2.5}$$

and

$$\Gamma_g \cap \Gamma_h = \emptyset, \tag{2.6}$$

where Γ_g and Γ_h represent the Dirichlet- and Neumann- type boundaries. Hence,

$$\mathbf{u}(\mathbf{x},t) = \mathbf{g}(\mathbf{x},t) \quad \text{on} \quad \Gamma_g \times [0,T] \tag{2.7}$$

$$\mathbf{n}.\sigma = \mathbf{h}(\mathbf{x},t) \quad \text{on} \quad \Gamma_h \times [0,T], \tag{2.8}$$

where $\mathbf{n}$ is the outward unit normal vector to Γ_h.

In the case of a pure Dirichlet problem ($\Gamma_h = \emptyset$), the specified boundary velocity must satisfy

$$\int_\Gamma \mathbf{g}.\mathbf{n} \quad d\Gamma = 0, \tag{2.9}$$

i.e, the net flux of matter through the boundary should be zero.

The initial condition associated to this problem is

$$\mathbf{u}(\mathbf{x},0) = \mathbf{u}_0(\mathbf{x}) \quad \text{on} \quad \Omega \tag{2.10}$$

For the well-posedness of the problem, the initial field must be divergence-free, i.e,

$$\nabla.\mathbf{u}_0 = 0 \tag{2.11}$$

We will see later the importance of the discrete counterpart of that condition in the solution process.

The system of eqns (2.1)-(2.2) and the associated boundary and initial conditions are called the velocity-pressure (or primitive variable) form of the Navier-Stokes equations.

2.2 The vorticity stream-function formulation

The vorticity transport equation can be obtained by taking the curl of the momentum equation,

$$\nabla \times \{\frac{\partial \mathbf{u}}{\partial t} + (\mathbf{u}.\nabla)\mathbf{u}\} = \nabla \times \{-\nabla p + \nu \nabla^2 \mathbf{u}\} \tag{2.12}$$

Now, we use the vector identity [13],

$$(\mathbf{u}.\nabla)\mathbf{u} = \frac{1}{2}\nabla|\mathbf{u}|^2 - \mathbf{u} \times (\nabla \times \mathbf{u}) \tag{2.13}$$

Replacing eqn (2.13) in eqn (2.12) and using the relations

$$\nabla \times \nabla|\mathbf{u}|^2 = 0 \tag{2.14}$$

$$\nabla \times \nabla p = 0 \tag{2.15}$$

$$\nabla^2 \mathbf{u} = -\nabla \times (\nabla \times \mathbf{u}) \tag{2.16}$$

(in eqn (2.16), we have used $\nabla.\mathbf{u} = 0$), we obtain

$$\frac{\partial(\nabla \times \mathbf{u})}{\partial t} - \nabla \times (\mathbf{u} \times \nabla \times \mathbf{u}) = -\nu \nabla \times \nabla \times \nabla \times \mathbf{u} \tag{2.17}$$

The vorticity is defined as

$$\omega = \nabla \times \mathbf{u} \tag{2.18}$$

By substitution of eqn (2.18) in eqn (2.17), we obtain the vorticity transport equation,

$$\frac{\partial \omega}{\partial t} + (\mathbf{u}.\nabla)\omega = (\omega.\nabla)\mathbf{u} + \nu \nabla^2 \omega \tag{2.19}$$

In the case of a two-dimensional flow, eqn (2.19) simplifies to

$$\frac{\partial \omega}{\partial t} + \mathbf{u}.\nabla\omega = \nu \nabla^2 \omega \tag{2.20}$$

The velocity $\mathbf{u}$ being solenoidal, there exists a vector field $\mathbf{\Psi} = (0, 0, \Psi)$ such that

$$\mathbf{u} = \nabla \times \mathbf{\Psi} \tag{2.21}$$

The nonzero component of $\mathbf{\Psi}$ is called the stream function. A relation between the vorticity and the stream function is obtained as

$$\begin{aligned} \omega &= \nabla \times \nabla \times \mathbf{\Psi} \\ &= -\nabla^2 \mathbf{\Psi} \end{aligned} \tag{2.22}$$

The vorticity stream-function form of the Navier-Stokes equations for two-dimensional flows is the set of coupled scalar equations given below :

$$\frac{\partial \omega}{\partial t} + \mathbf{u}.\nabla\omega = \nu\nabla^2\omega \qquad \text{on } \Omega \times [0, T] \tag{2.23}$$

$$\nabla^2\Psi = -\omega \qquad \text{on } \Omega \times [0, T] \tag{2.24}$$

where Ω is a domain of R^2, $\mathbf{u}(\mathbf{x}, t)$ is the velocity, $\omega(\mathbf{x}, t)$ is the vorticity, $\Psi(\mathbf{x}, t)$ is the stream function, and ν is the kinematic viscosity. The vorticity and the stream function are related to the velocity field through

$$\omega = \frac{\partial u_2}{\partial x_1} - \frac{\partial u_1}{\partial x_2} \tag{2.25}$$

$$u_1 = \frac{\partial \Psi}{\partial x_2} \tag{2.26}$$

$$u_2 = -\frac{\partial \Psi}{\partial x_1} \tag{2.27}$$

We assume that the boundary Γ of the domain Ω has the following decompositions:

$$\Gamma = \overline{\Gamma_g \cup \Gamma_G \cup \Gamma_h} \tag{2.28}$$

$$\emptyset = \Gamma_g \cap \Gamma_h \tag{2.29}$$

$$\emptyset = \Gamma_G \cap \Gamma_h \tag{2.30}$$

$$\emptyset = \Gamma_g \cap \Gamma_G \tag{2.31}$$

$$\Gamma = \overline{\Gamma_{\tilde{g}} \cup \Gamma_G \cup \Gamma_{\tilde{h}}} \tag{2.32}$$

$$\emptyset = \Gamma_{\tilde{g}} \cap \Gamma_{\tilde{h}} \tag{2.33}$$

$$\emptyset = \Gamma_G \cap \Gamma_{\tilde{h}} \tag{2.34}$$

$$\emptyset = \Gamma_{\tilde{g}} \cap \Gamma_G \tag{2.35}$$

where Γ_g and Γ_h represent Dirichlet- and Neuman-type boundaries for Ψ, $\Gamma_{\tilde{g}}$ and $\Gamma_{\tilde{h}}$ represent Dirichlet- and Neuman-type boundaries for ω, and Γ_G represents both Dirichlet- and Neuman-type boundaries for Ψ . Hence,

$$\Psi(\mathbf{x},t) = \Psi_g(\mathbf{x},t) \qquad \text{on } \Gamma_g \times [0,T] \tag{2.36}$$

$$\Psi(\mathbf{x},t) = \Psi_G(\mathbf{x},t) \qquad \text{on } \Gamma_G \times [0,T] \tag{2.37}$$

$$\mathbf{n}.\nabla\Psi(\mathbf{x},t) = u_\tau \qquad \text{on } \Gamma_G \times [0,T] \tag{2.38}$$

$$\mathbf{n}.\nabla\Psi(\mathbf{x},t) = h(\mathbf{x},t) \qquad \text{on } \Gamma_h \times [0,T] \tag{2.39}$$

$$\omega(\mathbf{x},t) = \omega_{\tilde{g}}(\mathbf{x},t) \qquad \text{on } \Gamma_{\tilde{g}} \times [0,T] \tag{2.40}$$

$$\nu\mathbf{n}.\nabla\omega(\mathbf{x},t) = \tilde{h}(\mathbf{x},t) \qquad \text{on } \Gamma_{\tilde{h}} \times [0,T] \tag{2.41}$$

The boundary Γ_G represents the solid surfaces in the flow domain. The initial condition for vorticity in eqn (2.23) is given as

$$\omega(\mathbf{x},0) = \omega_0(\mathbf{x}) \qquad \text{on } \Omega \tag{2.42}$$

Remarks :

1) In the case of a two-dimensional flow, the vorticity-stretching term $(\omega.\nabla)\mathbf{u}$ is zero and the vorticity transport equation contains only one nonlinear term. This, together with the scalar nature of the equations, is the reason why the vorticity stream-function formulation is very convenient in two dimensions.

2) The vorticity transport eqn (2.23) belongs to a large class of convection-diffusion problems . In this case, the transported quantity is the vorticity ω.

3) The flow field obtained from the solution of eqns (2.23) and (2.24) is divergence-free by construction.

4) For flow domains having solid boundaries (e.g., walls or obstacles) the no-slip and no-penetration conditions yield constraints on the derivatives of Ψ, i.e,

$$\mathbf{n}.\nabla\Psi = u_\tau \tag{2.43}$$

$$\tau.\nabla\Psi = 0 \tag{2.44}$$

where τ and $\mathbf{n}$ are the tangential and normal unit vectors at the surface whereas u_τ is the tangential component of the velocity at the wall. Moreover, the stream function assumes constant values along solid boundaries. However, it is difficult to derive any boundary condition for vorticity at solid surfaces. The boundary values of the vorticity at solid surfaces are related to the local boundary-layer profiles and are thus time dependent. On the other hand, they do not arise naturally from the no-slip and no-penetration conditions. A classical procedure to update the wall values of ω in multiply-connected domains is to include the solution of an auxiliary Poisson problem in a semi-implicit time integration scheme for eqns (2.23)-(2.24) [1]. An alternative approach to the numerical treatment of vorticity at no slip-boudaries is discussed in [2].

For flows in symmetrical domains having only one inner boundary, we propose [14] to take advantage of the time discretization of the problem to treat the wall values of ω as unknowns in the discrete Poisson equation arising from eqn (2.24). This process will be described in Chapter 3.

CHAPTER 3: NUMERICAL PROCEDURES FOR THE VORTICITY STREAM-FUNCTION FORMULATION

3.1 Variational formulation

In the sequel, we will use the Hilbert space

$$L_2(\Omega) = \{\Phi | \Phi \quad \text{is possibly discontinuous and} \quad \int_\Omega |\Phi|^2 d\Omega < +\infty\} \tag{3.1}$$

and the Sobolev space

$$H_1(\Omega) = \{\Phi | \Phi \in L_2(\Omega), \frac{\partial \Phi}{\partial x_i} \in L^2(\Omega), \forall i = 1,2\}. \tag{3.2}$$

We introduce the following spaces:

$$V(\Omega) = \{w | w \in H_1(\Omega), w = 0 \text{ on } \Gamma_g\} \tag{3.3}$$

$$S(\Omega) = \{\Psi | \Psi \in H_1(\Omega), \Psi = \Psi_g \text{ on } \Gamma_g, \Psi = \Psi_G \text{ on } \Gamma_G\} \tag{3.4}$$

$$\tilde{V}(\Omega) = \{w | w \in H_1(\Omega), w = 0 \text{ on } \Gamma_{\tilde{g}} \cup \Gamma_G\} \tag{3.5}$$

$$\tilde{S}(\Omega) = \{\omega | \omega \in H_1(\Omega), \omega = \omega_{\tilde{g}} \text{ on } \Gamma_{\tilde{g}}, \omega = \omega_G \text{ on} \Gamma_G\} \tag{3.6}$$

The variational form of the vorticity stream-function problem is the following: Find ω in $\tilde{S}(\Omega)$ such that for all w in $\tilde{V}$,

$$\int_\Omega w(\frac{\partial \omega}{\partial t} + \mathbf{u}.\nabla\omega)d\Omega + \int_\Omega \nu \nabla w.\nabla\omega d\Omega = \int_{\Gamma_h} w\tilde{h}d\Gamma \tag{3.7}$$

and find Ψ in $S(\Omega)$ such that for all w in $V(\Omega)$,

$$\int_\Omega \nabla w.\nabla\Psi d\Omega - \int_\Omega w\omega d\Omega = \int_{\Gamma_h} whd\Gamma + \int_{\Gamma_G} wu_\tau d\Gamma \tag{3.8}$$

3.2 Finite-element formulation

Let Q^h denote a finite-element discretization of the computational domain Ω into subdomains Ω^e , $e = 1, 2, ..., nel$, where nel is the number of elements. Let M be a vertex of Q^h . We assume

$$\bar{\Omega} = \bigcup_{e=1}^{nel} \bar{\Omega}^e \tag{3.9}$$

$$\emptyset = \bigcap_{e=1}^{nel} \Omega^e \tag{3.10}$$

We associate to Q^h the finite dimensional spaces,

$$H_1^h(\Omega) = \{\Phi^h | \Phi^h \in C^0(\Omega), \Phi^h|_{\Omega^e} \in P^1, \forall \Omega^e \in Q^h\}, \tag{3.11}$$

where P^1 is the space of first order polynomials in x_1, x_2,

$$V^h(\Omega) = \{w^h | w^h \in H_1^h(\Omega), w^h \simeq 0 \text{ on } \Gamma_g\}, \tag{3.12}$$

$$S^h(\Omega) = \{\Psi^h | \Psi^h \in H_1^h(\Omega), \Psi^h \simeq \Psi_g \text{ on } \Gamma_g, \Psi^h \simeq \Psi_G \text{ on } \Gamma_G\}, \tag{3.13}$$

$$\tilde{V}^h(\Omega) = \{w^h | w^h \in H_1^h(\Omega), w^h \simeq 0 \text{ on } \Gamma_{\tilde{g}} \cup \Gamma_G\}, \tag{3.14}$$

$$\tilde{S}^h(\Omega) = \{\omega^h | \omega^h \in H_1^h(\Omega), \omega^h \simeq \omega_{\tilde{g}} \text{ on } \Gamma_{\tilde{g}}, \omega^h \simeq \omega_G \text{ on} \Gamma_G\}. \tag{3.15}$$

In the above definitions, we assume that Ψ_g, $\omega_{\tilde{g}}$ and ω_G are known quantities. The discrete variational problem associated with eqn (3.15) is given as follows: Find ω^h in $\tilde{S}^h(\Omega)$, such that for all w^h in $\tilde{V}^h$

$$\int_\Omega w^h (\frac{\partial \omega^h}{\partial t} + \mathbf{u}.\nabla\omega^h) d\Omega + \int_\Omega \nu \nabla w^h . \nabla \omega^h d\Omega +$$
$$\sum_{e=1}^{Nel} \int_{\Omega^e} \delta (\frac{\partial \omega^h}{\partial t} + \mathbf{u}.\nabla\omega^h - \nu\nabla^2\omega^h) d\Omega = \int_{\Gamma_h} w^h \tilde{h} d\Gamma \tag{3.16}$$

where δ is a $C^{-1}(\Omega)$ perturbation to the weighting function w^h. The selection of the Petrov-Galerkin perturbation will be further addressed in Section 3.4. Based on ω^h (solution of eqn (3.16)) we define the following space:

$$S_G^h(\Omega) = \{\omega_*^h | \omega_*^h \in H_1^h(\Omega), \omega_*^h(M) = \omega^h(M) \text{ if } M \notin \Gamma_G\} \tag{3.17}$$

The discrete variational form associated with eqn (3.8) can be stated as follows: Find $\Psi^h \in S^h$,and $\omega_*^h \in S_G^h$ such that for all $w^h \in V^h$

$$\int_\Omega \nabla w^h . \nabla \Psi^h d\Omega - \int_\Omega w^h \omega_*^h d\Omega = \int_{\Gamma_h} w^h h d\Gamma + \int_{\Gamma_G} w^h u_\tau d\Gamma \tag{3.18}$$

Remarks :

1) Note that if $\delta = 0$ we have a Galerkin formulation; if $\delta \neq 0$ we have a Petrov-Galerkin formulation. The perturbation weights only the element interiors and does not affect the boundary terms.

2) Brooks and Hughes [8] have shown that in the case of general convection-diffusion problems, for rectangular elements , the perturbation does not affect the weighting of the diffusion term, and for reasonable element shapes the contribution is expected to be negligible.

3.3 Temporal discretization

The system of ordinary differential equations obtained from eqns(3.16)-(3.18) is

$$\mathbf{Ma} + \mathbf{Cv} = \mathbf{F} \tag{3.19}$$

$$\mathbf{v}(0) = \mathbf{v}_0 \tag{3.20}$$

$$\mathbf{Kd} - \mathbf{Mv}_* = \mathbf{E} \tag{3.21}$$

where $\mathbf{v}$ is the vector of nodal values of ω^h and $\mathbf{a}$ is its time derivative, whereas $\mathbf{d}$ is the vector of nodal values of Ψ^h and $\mathbf{v}_*$ is the vector of nodal values of ω_*^h. In eqns(3.19)-(3.21), $\mathbf{M}$ is the mass matrix, $\mathbf{C}$ is the sum of the diffusion matrix and the linearized convection operator, $\mathbf{K}$ is the discrete Laplace operator ; $\mathbf{F}$ and $\mathbf{E}$ are generalized force vectors containing the fluxes and the specified values at the boundary.

This system is solved with the following semi-implicit predictor/multi-corrector algorithm [8]:

i) Initialization: $\mathbf{v}_n, \mathbf{a}_n, \mathbf{d}_n$ are known. If $n = 0$, the initial conditions are used.

ii) Prediction:

$$\mathbf{v}_{n+1}^0 = \mathbf{v}_n + (1-\gamma)\Delta t \mathbf{a}_n \tag{3.22}$$

$$\mathbf{a}_{n+1}^0 = \mathbf{0} \tag{3.23}$$

$$\mathbf{Kd}_{n+1}^0 - \mathbf{Mv}_{*n+1}^0 = \mathbf{E}_{n+1} \tag{3.24}$$

$$\mathbf{u}_{n+1}^0 = \left(\frac{\partial \Psi_{n+1}^0}{\partial x_1}, \frac{-\partial \Psi_{n+1}^0}{\partial x_2}\right) \tag{3.25}$$

Here Δt is the time step and γ $(0. < \gamma < 1.)$ is a parameter governing the stability and accuracy of the integration scheme.

iii) Correction:

$$\mathbf{M}^* \Delta \mathbf{a}^i_{n+1} = \mathbf{F}_{n+1} - \mathbf{M}\mathbf{a}^i_{n+1} - \mathbf{C}\mathbf{v}^i_{n+1} = \mathbf{R}^i_{n+1} \tag{3.26}$$

$$\text{with } \mathbf{M}^* = (\mathbf{M} + \gamma \Delta t \mathbf{C}) \tag{3.27}$$

$$\mathbf{v}^{i+1}_{n+1} = \mathbf{v}^i_{n=1} + \gamma \Delta t \Delta \mathbf{a}^i_{n+1} \tag{3.28}$$

$$\mathbf{a}^{i+1}_{n+1} = \mathbf{a}^i_{n+1} + \Delta \mathbf{a}^i_{n+1} \tag{3.29}$$

$$\mathbf{K}\mathbf{d}^{i+1}_{n+1} - \mathbf{M}\mathbf{v}^{i+1}_{*n+1} = \mathbf{E}_{n+1} \tag{3.30}$$

$$\mathbf{u}^{i+1}_{n+1} = \left(\frac{\partial \Psi^{i+1}_{n+1}}{\partial x_2}, -\frac{\partial \Psi^{i+1}_{n+1}}{\partial x_1}\right) \tag{3.31}$$

The iterations continue until the L^h_2 norm of the residual $\mathbf{R}^{i+1}_{n+1}$ becomes smaller than a predetermined error tolerance.

3.4 Selection of the Petrov-Galerkin perturbation

In the present study, we have used a streamline-upwind/Petrov-Galerkin procedure. In this formulation, the perturbation to the shape function is given as

$$\delta = C_{2\tau} z \frac{h}{2} \mathbf{s}.\nabla N_a, \tag{3.32}$$

where

$C_{2\tau}$ is the algorithmic Courant number [11],

$\mathbf{s} = \dfrac{\mathbf{u}}{\|\mathbf{u}\|}$ is a vector of unit length pointing in the advection direction,

h is the element length,

z is a function of the element Peclet number Pe given as [8]

$$z(Pe) = \begin{cases} \frac{1}{3} Pe & \text{if } 0 \le Pe \le 3 \\ 1 & \text{if } Pe > 3 \end{cases}$$

where $Pe = \|\mathbf{u}\| \dfrac{h}{2\nu}$ is the element Peclet number.

Various selections for $C_{2\tau}$ and their stability/accuracy properties are discussed in [11]. In the present study, we have used

$$C_{2\tau} = 1 \tag{3.33}$$

and

$$C_{2\tau} = C_{\Delta t} \tag{3.34}$$

where

$$C_{\Delta t} = \frac{\Delta t \|\mathbf{u}\|}{h} \tag{3.35}$$

is the element Courant number.

These selections of the Petrov-Galerkin perturbation are such that the scheme introduces a certain amount of artificial diffusion in the convection direction, but induces minimal such diffusion in the cross-convection direction. This method can be recast in terms of the use of an additional anisotropic diffusion tensor [8] added to the physical one which is isotropic in the case of Newtonian fluids. Such procedures have also been introduced through the use of a generalized governing equation [15] obtained by subtracting from the original differential equation the scalar product of its gradient by a vector of free parameters associated to each of the coordinate directions.

All the so-called Petrov-Galerkin formulations are intended to prevent the occurence of oscillations in the computed flow field. Such oscillations in the solution can be obtained when regular Galerkin formulations are used. Typically, in the presence of shocks or boudary layers, if the mesh is not fine enough to resolve the discontinuity and sharp gradients, the solution might be oscillatory. Usually, the oscillations in the solutions can be avoided by a mesh refinment where the mesh spacing is set smaller than the boundary layer thickness [16]. However, this approach can lead to a dramatic increase in the number of nodal points. The size of the problem is then likely to become very large, especially for three-dimensional simulations. The use of Petrov-Galerkin formulations is an alternative to mesh refinment for obtaining accurate wiggle-free solutions in a cost-effective way.

CHAPTER 4: NUMERICAL PROCEDURES FOR THE PRIMITIVE VARIABLE FORMULATION

4.1 Variational formulation

Using the definition of $H_1(\Omega)$ introduced in Section 3.1, we define the following spaces:

$$V(\Omega) = \{\mathbf{w} | \mathbf{w} \in H_1(\Omega) \times H_1(\Omega), \mathbf{w} = \mathbf{0} \quad \text{on} \quad \Gamma_g\} \tag{4.1}$$

$$S(\Omega) = \{\mathbf{u} | \mathbf{u} \in H_1(\Omega) \times H_1(\Omega), \mathbf{u} = \mathbf{g} \quad \text{on} \quad \Gamma_g\} \tag{4.2}$$

The variational form of the problem defined by eqns (2.1)-(2.2) can be stated as follows : Find $\mathbf{u} \in S(\Omega)$ and $p \in H_1(\Omega)$, such that for all $\mathbf{w} \in V(\Omega)$ and for all $q \in H_1(\Omega)$,

$$\int_\Omega \mathbf{w} \frac{\partial \mathbf{u}}{\partial t} d\Omega + \int_\Omega \mathbf{w}(\mathbf{u}.\nabla)\mathbf{u} d\Omega = \int_\Omega \mathbf{w} \nabla.\sigma d\Omega \tag{4.3}$$

and

$$\int_\Omega q \nabla.\mathbf{u} d\Omega = 0 \tag{4.4}$$

Note that

$$\begin{aligned} \int_\Omega \mathbf{w} \nabla.\sigma d\Omega &= \int_\Omega \nabla.(\mathbf{w}\sigma) d\Omega - \int_\Omega \sigma.\nabla \mathbf{w} d\Omega \\ &= \int_\Gamma \mathbf{w}.(\mathbf{n}.\sigma) d\Gamma - \int_\Omega \sigma.\nabla \mathbf{w} d\Omega \end{aligned} \tag{4.5}$$

So eqn (4.3) can be rewritten as

$$\int_\Omega \mathbf{w} \frac{\partial \mathbf{u}}{\partial t} d\Omega + \int_\Omega \mathbf{w}(\mathbf{u}.\nabla)\mathbf{u} d\Omega = \int_{\Gamma_h} \mathbf{w}.(\mathbf{n}.\sigma) d\Gamma - \int_\Omega \sigma.\nabla \mathbf{w} d\Omega \tag{4.6}$$

Moreover,

$$\begin{aligned} \sigma.\nabla \mathbf{w} &= -p\mathbf{I}.\nabla \mathbf{w} + 2\nu\varepsilon(\mathbf{u})\nabla \mathbf{w} \\ &= -p\nabla.\mathbf{w} + 2\nu\varepsilon(\mathbf{u})\varepsilon(\mathbf{w}) \end{aligned} \tag{4.7}$$

We obtain

$$\begin{aligned} &\int_\Omega \mathbf{w} \frac{\partial \mathbf{u}}{\partial t} d\Omega + \int_\Omega \mathbf{w}(\mathbf{u}.\nabla)\mathbf{u} d\Omega - \int_\Omega p\nabla.\mathbf{w} d\Omega \\ &+ \int_\Omega 2\nu\varepsilon(\mathbf{w})\varepsilon(\mathbf{u}) d\Omega = \int_{\Gamma_h} \mathbf{w}.(\mathbf{n}.\sigma) d\Gamma \end{aligned} \tag{4.8}$$

Using the boundary condition (2.8), we get

$$\int_\Omega \mathbf{w}\frac{\partial \mathbf{u}}{\partial t}d\Omega + \int_\Omega \mathbf{w}(\mathbf{u}.\nabla)\mathbf{u}d\Omega - \int_\Omega p\nabla.\mathbf{w}d\Omega$$
$$+ \int_\Omega 2\nu\epsilon(\mathbf{w})\epsilon(\mathbf{u})d\Omega = \int_{\Gamma_h} \mathbf{w}.\mathbf{h}d\Gamma \tag{4.9}$$

The variational form of the continuous problem (2.1)-(2.2) is given by eqns (4.4) and (4.9).

The initial condition associated to the variational problem is

$$\int_\Omega \mathbf{w}\{\mathbf{u}(\mathbf{x},0) - \mathbf{u}_0(\mathbf{x})\}d\Omega = 0 \tag{4.10}$$

4.2 Finite-element formulation

Let Q^h denote a finite-element discretization of the computational domain Ω into subdomains $\Omega^e, e = 1, ..., nel$ where nel is the number of elements. We assume

$$\bar{\Omega} = \bigcup_{e=1}^{nel} \bar{\Omega}^e \tag{4.11}$$

$$\emptyset = \bigcap_{e=1}^{nel} \Omega^e \tag{4.12}$$

To obtain a discrete variational problem, the functions $\mathbf{w}, \mathbf{u}, p, q$ are approximated by piecewise polynomial functions $\mathbf{w}^h, \mathbf{u}^h, p^h, q^h$; so, we introduce the following finite dimensional spaces:

$$V^h(\Omega) = \{\mathbf{w}^h | \mathbf{w}^h \in H_1(\Omega) \times H_1(\Omega), \mathbf{w}^h|_{\Omega^e} \in P^\alpha, \mathbf{w}^h|_{\Gamma_g} = 0\} \tag{4.13}$$

$$S^h(\Omega) = \{\mathbf{u}^h | \mathbf{u}^h \in H_1(\Omega) \times H_1(\Omega), \mathbf{u}^h|_{\Omega^e} \in P^\alpha, \mathbf{u}^h|_{\Gamma_g} = \mathbf{g}^h\} \tag{4.14}$$

$$H_1^h(\Omega) = \{q^h | q^h \in H_1(\Omega), q^h|_{\Omega^e} \in P^\beta\} \tag{4.15}$$

where P^α (resp. P^β) is the set of piecewise polynomial functions of order α (resp. β). The selection of the order of the polynomial interpolants will be discussed in the sequel.

The Petrov-Galerkin variational form of eqns (4.9) and (4.4) is the following: Find $\mathbf{u}^h \in S^h(\Omega)$ and $p^h \in H_1^h(\Omega)$, such that for all $\mathbf{w}^h \in V^h(\Omega)$ and for all $q^h \in H_1^h$,

$$\int_\Omega \mathbf{w}^h \frac{\partial \mathbf{u}^h}{\partial t} d\Omega + \int_\Omega \mathbf{w}^h(\mathbf{u}^h.\nabla \mathbf{u}^h) d\Omega + 2\nu \int_\Omega \varepsilon(\mathbf{w}^h)\varepsilon(\mathbf{u}^h) d\Omega - \int_\Omega p^h \nabla.\mathbf{w}^h d\Omega +$$
$$\sum_{e=1}^{nel} \int_{\Omega^e} \delta(\frac{\partial \mathbf{u}^h}{\partial t} + \mathbf{u}.\nabla \mathbf{u}^h - \nabla \sigma^h) d\Omega = \int_{\Gamma_h} \mathbf{w}^h \mathbf{h} d\Gamma \tag{4.16}$$

$$\int_\Omega q^h \nabla.\mathbf{u}^h d\Omega = 0 \tag{4.17}$$

where δ is a $C^{-1}(\Omega)$ perturbation. The selection of the Petrov- Galerkin perturbation will be discussed later. Note that if $\delta = 0$, we have a Galerkin formulation; if $\delta \neq 0$, we have a Petrov-Galerkin formulation.

We can rewrite eqn (4.16) as

$$\int_\Omega \tilde{\mathbf{w}}^h \frac{\partial \mathbf{u}^h}{\partial t} d\Omega + \int_\Omega \tilde{\mathbf{w}}^h \mathbf{u}^h.\nabla \mathbf{u}^h d\Omega + 2\nu \int_\Omega \varepsilon(\mathbf{w}^h)\varepsilon(\mathbf{u}^h) d\Omega$$
$$- \int_\Omega p^h \nabla.\mathbf{w}^h d\Omega - \sum_{e=1}^{nel} \int_{\Omega^e} \delta \nabla.\sigma^h = \int_{\Gamma_h} \mathbf{w}^h \mathbf{h} d\Gamma \tag{4.18}$$

where $\tilde{\mathbf{w}}^h = \mathbf{w}^h + \delta$. In the sequel we will assume that the contribution of the Petrov-Galerkin perturbation to the stress-divergence term (the last term on the left-hand-side) is negligible.

4.3 Temporal discretization

4.3.1 Time-integration scheme

The discrete eqns (4.16)-(4.17) have the following equivalent matrix form:

$$\mathbf{M}\dot{\mathbf{v}} + \mathbf{N}(\mathbf{v}) + \mathbf{C}\mathbf{v} - \mathbf{G}\mathbf{p} = \mathbf{F} \tag{4.19}$$

$$\mathbf{G}^\mathbf{T}\mathbf{v} = \mathbf{D} \tag{4.20}$$

where $\mathbf{v}$ is the vector of unknown nodal values of the discrete velocity field, $\dot{\mathbf{v}}$ is its time derivative and $\mathbf{p}$ is the vector of unknown nodal values for the discrete pressure field. $\mathbf{M}$ is the mass matrix, $\mathbf{N}(\mathbf{v})$ is the nonlinear convection vector, $\mathbf{C}$ is the diffusion matrix, $\mathbf{G}$ is the discrete gradient operator. $\mathbf{F}$ and $\mathbf{D}$ are generalized force vectors containing the prescribed fluxes and displacements.

The time integration of this system is obtained through the following predictor-multicorrector algorithm [8]:

1) Initialization:

$$\mathbf{v}_n, \quad \dot{\mathbf{v}}_n, \quad \mathbf{p}_n \text{ are known.}$$

If $n = 0$, the initial conditions $\mathbf{v}_0$ and $\dot{\mathbf{v}}_0$ are used. In the continuous problem, there is no initial condition required for the pressure, and neither is there any in the discrete problem. However, as will be shown later, the initial discrete velocity field must satisfy the approximate incompressibility constraint,

$$\mathbf{G}^{\mathbf{T}}\mathbf{v}_0 = \mathbf{0} \tag{4.21}$$

2) Prediction :

$$\mathbf{v}_{n+1}^0 = \mathbf{v}_n + (1-\gamma)\Delta t\dot{\mathbf{v}}_n \tag{4.22}$$

$$\dot{\mathbf{v}}_{n+1}^0 = \mathbf{0} \tag{4.23}$$

where the definitions of Δt and γ are the same as in Section 3.3.

3) Correction :

$$\mathbf{M}\dot{\mathbf{v}}_{n+1}^{i+1} + \mathbf{N}(\mathbf{v}_{n+1}^{i+1}) + \mathbf{C}\mathbf{v}_{n+1}^{i+1} - \mathbf{G}\mathbf{p}_{n+1}^{i+1} = \mathbf{F}_{n+1} \tag{4.24}$$

$$\mathbf{G}^{\mathbf{T}}\mathbf{v}_{n+1}^{i+1} = \mathbf{D}_{n+1} \tag{4.25}$$

We introduce the incremental forms given below:

$$\dot{\mathbf{v}}_{n+1}^{i+1} = \dot{\mathbf{v}}_{n+1}^{i} + \Delta\dot{\mathbf{v}}_{n+1}^{i} \tag{4.26}$$

$$\mathbf{v}_{n+1}^{i+1} = \mathbf{v}_{n+1}^{i} + \Delta\mathbf{v}_{n+1}^{i} \tag{4.27}$$

$$\mathbf{p}_{n+1}^{i+1} = \mathbf{p}_{n+1}^{i} + \Delta\mathbf{p}_{n+1}^{i} \tag{4.28}$$

Substituting eqns (4.26),(4.27) and (4.28) into eqn (4.24) yields

$$\begin{aligned}&\mathbf{M}\dot{\mathbf{v}}_{n+1}^{i} + \mathbf{N}(\mathbf{v}_{n+1}^{i} + \Delta\mathbf{v}_{n+1}^{i}) + \mathbf{C}\mathbf{v}_{n+1}^{i} - \mathbf{G}\mathbf{p}_{n+1}^{i} \\ &+ \mathbf{M}\Delta\dot{\mathbf{v}}_{n+1}^{i} + \mathbf{C}\Delta\mathbf{v}_{n+1}^{i} - \mathbf{G}\Delta\mathbf{p}_{n+1}^{i} = \mathbf{F}_{n+1}\end{aligned} \tag{4.29}$$

A Taylor expansion of the vector $\mathbf{N}(\mathbf{v}_{n+1}^{i} + \Delta\mathbf{v}_{n+1}^{i})$ in the vicinity of $\mathbf{v}_{n+1}^{i}$ yields

$$\mathbf{N}(\mathbf{v}_{n+1}^{i} + \Delta\mathbf{v}_{n+1}^{i}) \simeq \mathbf{N}(\mathbf{v}_{n+1}^{i}) + \frac{\partial\mathbf{N}}{\partial\mathbf{v}}\Big|_{\mathbf{v}_{n+1}^{i}}\Delta\mathbf{v}_{n+1}^{i} \tag{4.30}$$

From eqns (4.29) and (4.30) we obtain

$$\begin{aligned}&\mathbf{M}\Delta\dot{\mathbf{v}}_{n+1}^{i} + \frac{\partial\mathbf{N}}{\partial\mathbf{v}}\Big|_{\mathbf{v}_{n+1}^{i}}\Delta\mathbf{v}_{n+1}^{i} + \mathbf{C}\Delta\mathbf{v}_{n+1}^{i} - \mathbf{G}\Delta\mathbf{p}_{n+1}^{i} \\ &= \mathbf{F}_{n+1} - \{\mathbf{M}\dot{\mathbf{v}}_{n+1}^{i} + \mathbf{N}(\mathbf{v}_{n+1}^{i}) + \mathbf{C}\mathbf{v}_{n+1}^{i} - \mathbf{G}\mathbf{p}_{n+1}^{i}\}\end{aligned} \tag{4.31}$$

Let

$$\mathbf{R}^i_{n+1} = \mathbf{F}_{n+1} - \{\mathbf{M}\dot{\mathbf{v}}^i_{n+1} + \mathbf{N}(\mathbf{v}^i_{n+1}) + \mathbf{C}\mathbf{v}^i_{n+1} - \mathbf{G}\mathbf{p}^i_{n+1}\} \tag{4.32}$$

On the other hand,

$$\Delta\mathbf{v}^{i+1}_{n+1} = \gamma\Delta t\Delta\dot{\mathbf{v}}^i_{n+1}; \tag{4.33}$$

so, eqn (4.31) can be rewritten

$$[\mathbf{M} + \gamma\Delta t(\frac{\partial\mathbf{N}}{\partial\mathbf{v}}|_{\mathbf{v}^i_{n+1}} + \mathbf{C})]\Delta\dot{\mathbf{v}}^i_{n+1} - \mathbf{G}\Delta\mathbf{p}^i_{n+1} = \mathbf{R}^i_{n+1} \tag{4.34}$$

The discrete continuity equation reads

$$\mathbf{G}^\mathbf{T}\Delta\mathbf{v}^i_{n+1} = \mathbf{D}_{n+1} - \mathbf{G}^\mathbf{T}\mathbf{v}^i_{n+1} \tag{4.35}$$

or

$$\mathbf{G}^\mathbf{T}\Delta\dot{\mathbf{v}}^i_{n+1} = \frac{1}{\gamma\Delta t}(\mathbf{D}_{n+1} - \mathbf{G}^\mathbf{T}\mathbf{v}^i_{n+1}) \tag{4.36}$$

Let

$$\mathbf{B}^i_{n+1} = \frac{1}{\gamma\Delta t}(\mathbf{D}_{n+1} - \mathbf{G}^\mathbf{T}\mathbf{v}^i_{n+1}) \tag{4.37}$$

Let

$$\mathbf{A} = \mathbf{M} + \gamma\Delta t(\frac{\partial\mathbf{N}}{\partial\mathbf{v}}|_{\mathbf{v}^i_{n+1}} + \mathbf{C}) \tag{4.38}$$

The residual form of the equation system (4.19)-(4.20) is

$$\mathbf{A}\Delta\dot{\mathbf{v}}^i_{n+1} - \mathbf{G}\mathbf{p}^i_{n+1} = \mathbf{R}^i_{n+1} \tag{4.39}$$

$$\mathbf{G}^\mathbf{T}\Delta\dot{\mathbf{v}}^i_{n+1} = \mathbf{B}^i_{n+1} \tag{4.40}$$

If $\Delta\dot{\mathbf{v}}^i_{n+1}$ and $\Delta\mathbf{p}^i_{n+1}$ are obtained by solving eqns (4.39)-(4.40), then the scheme is implicit. In the present formulation, an explicit scheme is used for the discrete momentum equation. Let

$$\mathbf{M}^* = \mathbf{M}^\mathbf{L} \tag{4.41}$$

be the lumped counterpart of $\mathbf{M}$ obtained by a column-sum technique. The matrix $\mathbf{M}^*$ replaces $\mathbf{A}$ in eqn (4.39) and we end up with the system,

$$\mathbf{M}^*\Delta\dot{\mathbf{v}}^i_{n+1} - \mathbf{G}^\mathbf{T}\Delta\mathbf{p}^i_{n+1} = \mathbf{R}^i_{n+1} \tag{4.42}$$

$$\mathbf{G}^\mathbf{T}\Delta\dot{\mathbf{v}}^i_{n+1} = \mathbf{B}^i_{n+1} \tag{4.43}$$

The following change of variable is introduced [8],

$$\Delta\dot{\mathbf{v}}^{*i}_{n+1} = \Delta\dot{\mathbf{v}}^i_{n+1} - \mathbf{M}^{*-1}\mathbf{G}\Delta\mathbf{p}^i_{n+1} \tag{4.44}$$

Eqn (4.42) reduces to

$$\mathbf{M}^{*}\Delta\dot{\mathbf{v}}^{*i}_{n+1} = \mathbf{R}^{i}_{n+1} \tag{4.45}$$

Replacing eqn (4.44) in eqn (4.43), we obtain an equation for $\Delta\mathbf{p}^{i}_{n+1}$ as

$$\mathbf{G}^{\mathbf{T}}\mathbf{M}^{*-1}\mathbf{G}\Delta\mathbf{p}^{i}_{n+1} = \mathbf{B}^{i}_{n+1} - \mathbf{G}^{\mathbf{T}}\Delta\dot{\mathbf{v}}^{*i}_{n+1} \tag{4.46}$$

Now, let $\mathbf{K} = \mathbf{G}^{\mathbf{T}}\mathbf{M}^{*-1}\mathbf{G}$. The pressure increment is obtained from

$$\mathbf{K}\Delta\mathbf{p}^{i}_{n+1} = \mathbf{B}^{i}_{n+1} - \mathbf{G}^{\mathbf{T}}\Delta\dot{\mathbf{v}}^{*i}_{n+1} \tag{4.47}$$

The complete acceleration increment is recovered from eqn (4.44) through

$$\Delta\dot{\mathbf{v}}^{i}_{n+1} = \Delta\dot{\mathbf{v}}^{*i}_{n+1} + \mathbf{M}^{*-1}\mathbf{G}\Delta\mathbf{p}^{i}_{n+1} \tag{4.48}$$

The discrete velocity and pressure fields are obtained from eqns (4.27)- (4.28).

The use of mass-lumping has many advantages. The left-hand-side matrix becomes diagonal and the storage required is reduced to a vector of length equal to the number of equations. Moreover the solution of the momentum eqn (4.45) can be obtained through a scalar product of vectors. This is an important asset in the framework of vectorization, because vector manipulations are among the fastest operations on supercomputers. Of course the use of an explicit scheme is expected to reduce the convergence rate of the solution. However, the increased number of iterations is fully compensated by the gain in storage. On the other hand, the matrix **K** is symmetric and the solution of the pressure equation can then be obtained through conjugate gradient type techniques. Note that **K** is not obtained by a classical assembly of element-level matrices but rather by mapping of element-level products into their location in the global matrix.

The reduction in storage requirements introduced by the use of an explicit treatment of the momentum equation is very important regarding the extension of the code to three dimensions. In that case, the study of practical problems involves solution of systems too large to allow the use of implicit algorithms. Owing to the implicit nature of the pressure, the discrete continuity equation cannot be solved by an explicit technique. However, the storage required for the matrix **K** is small with respect to that required for **A** (if the momentum equation was solved implicitly) because the pressure is a scalar quantity and because the order of interpolation of the pressure is less than that of the velocity. There are far fewer unknowns for the pressure than for the velocity and the size of **K** is much smaller than the size of **A**.

4.3.2 Selection of the initial condition

From a mathematical point of view, for the well-posedness of the problem, it is fundamental to have a divergence-free initial flow field [5], ie,

$$\nabla.\mathbf{u}_0 = \mathbf{0} \tag{4.49}$$

From a numerical point of view, this condition translates to

$$\mathbf{G}^{\mathbf{T}}\mathbf{v}_0 = \mathbf{0} \tag{4.50}$$

that is the discrete initial flow field should satisfy the discrete incompressibility condition. Failure to satisfy this constraint can lead to nonconverging solutions. In fact, suppose

$$\mathbf{G}^{\mathbf{T}}\mathbf{v}_0 \neq \mathbf{0} \text{ and } \dot{\mathbf{v}}_0 = \mathbf{0}; \tag{4.51}$$

then, the prediction step gives

$$\mathbf{v}_1^0 = \mathbf{v}_0 \tag{4.52}$$

$$\dot{\mathbf{v}}_1^0 = \mathbf{0} \tag{4.53}$$

After the first iteration, the discrete velocity field is

$$\mathbf{v}_1^1 = \mathbf{v}_1^0 + \gamma\Delta t(\Delta\dot{\mathbf{v}}_1^{*1} + \mathbf{M}^{*-1}\mathbf{G}\Delta\mathbf{p}_1^1) \tag{4.54}$$

where $\Delta\dot{\mathbf{v}}_1^{*1}$ is the solution of the discrete momentum equation at the first iteration, and $\Delta\mathbf{p}_1^1$ is the unknown pressure increment. Because we require $\mathbf{G}^{\mathbf{T}}\mathbf{v}_1^1 = \mathbf{0}$, we obtain

$$\mathbf{G}^{\mathbf{T}}\mathbf{v}_1^1 = \mathbf{G}^{\mathbf{T}}\mathbf{v}_1^0 + \gamma\Delta t\mathbf{G}^{\mathbf{T}}\Delta\dot{\mathbf{v}}_1^{*1} + \gamma\Delta t\mathbf{G}^{\mathbf{T}}\mathbf{M}^{*-1}\mathbf{G}\Delta\mathbf{p}_1^1 = \mathbf{0} \tag{4.55}$$

or

$$\begin{aligned}\mathbf{K}\Delta\mathbf{p}_1^0 &= \frac{-1}{\gamma\Delta t}\mathbf{G}^{\mathbf{T}}\mathbf{v}_1^0 - \mathbf{G}^{\mathbf{T}}\Delta\dot{\mathbf{v}}_1^{*1} \\ &= \frac{-1}{\gamma\Delta t}\mathbf{G}^{\mathbf{T}}\mathbf{v}_0 - \mathbf{G}^{\mathbf{T}}\Delta\dot{\mathbf{v}}_1^{*1}\end{aligned} \tag{4.56}$$

So if $\mathbf{G}^{\mathbf{T}}\mathbf{v}_0 \neq \mathbf{0}$, the right-hand side of the discrete Poisson equation varies like Δt^{-1}. This can produce the nonconvergence of the algorithm. However, it is not easy to specify an initial flow field satisfying the discrete incompressibility constraint. In the present study, we started the computations with an arbitrary convenient initial condition, typically $\mathbf{v}_0 = \mathbf{0}$ except on the Dirichlet boundaries. After one time step, the solution is such that $\mathbf{G}^{\mathbf{T}}\mathbf{v}_1 = \mathbf{0}$, but the pressure field is ususally erroneous. So because we have no initial condition for $\mathbf{p}$, we set it to zero and use $\mathbf{v}_1$ as an effective initial condition.

4.4 Selection of the Petrov-Galerkin perturbation

As for the vorticity stream-function formulation, we have used a streamline-upwind/Petrov-Galerkin scheme. In this scheme, the perturbation is again of the form,

$$\delta = C_{2\tau}z\frac{h}{2}\mathbf{s}.\nabla N_a, \tag{4.57}$$

with the definitions of Section 3.4 except for z. Here, we have taken

$$z = \coth(\frac{Pe}{4}) - \frac{4}{Pe} \tag{4.58}$$

This expression is an approximation of the formula given in [15] for the nine-node Lagrange element in two dimensions.

4.5 Selection of a mixed finite-element interpolation

4.5.1 Problem statement

In the primitive variable formulation of the Navier-Stokes equations, the orders of interpolation for velocity and pressure α and β cannot be selected arbitrarily. The problem can be set in the following terms:

The discrete equation,

$$\mathbf{Gp} = \mathbf{0}, \tag{4.59}$$

should have the unique solution $\mathbf{p} = \mathbf{0}$. Here $\mathbf{p}$ is the vector of nodal pressures, and $\mathbf{G}$ is the discrete gradient operator. Recall that the construction of the discrete gradient operator involves products of functions coming from the pressure and velocity spaces. The nonzero solutions of eqn(4.59), if they exist are called spurious pressure modes. They can be picked-up in the solution process and pollute the pressure field. However their presence does not affect the velocity solution. In fact, assume that $(\mathbf{u}, \mathbf{p})$ is one solution of the discrete system (4.19)- (4.20), then $(\mathbf{u}, \mathbf{p} + \mathbf{p}_s)$ with $\mathbf{p}_s \neq \mathbf{0}$ satisfying $\mathbf{Gp}_s = \mathbf{0}$ is also a solution.

Equal orders of interpolation for velocity and pressure, i.e, $\alpha = \beta$ are known to produce such spurious pressure modes. The usual cure is to use mixed finite -element interpolations, typically by interpolating the velocity with a polynomial function of degree higher than that used to interpolate the pressure. The two most usual combinations are bilinear velocity ($\alpha = 1$)/constant pressure ($\beta = 0$) and quadratic velocity ($\alpha = 2$)/bilinear pressure ($\beta = 1$). However, the bilinear velocity/constant pressure formulation has been used with mixed success [6,17]. In particular, it has been reported to produce spurious pressure modes under certain boundary conditions.

For the present work, we have chosen to use a quadratic velocity/bilinear pressure formulation.

4.5.2 The four-node + bubble element

The first element we have used in the computations is a bilinear + bubble velocity/bilinear pressure element. It contains five nodal points for velocity, one at each of the four vertices of the quadrilateral and one at the center of the element. The four nodes for the pressure are at the four vertices of the element (Figure 4.1). This element is not usual for the solution of the Navier-Stokes equations. Our goal when selecting it was to use a mixed interpolation of the type quadratic velocity/bilinear pressure while reducing the cost associated with the computation of the element level arrays. In fact, in that situation, the number of velocity unknowns is 10 for each interior element; thus, the element level arrays such as mass, diffusion and convection matrices are 10×10 matrices. The element level gradient operator is a 10×4 array. However, this element is only an extension of a bilinear velocity/bilinear pressure element and is not totally free of the drawbacks

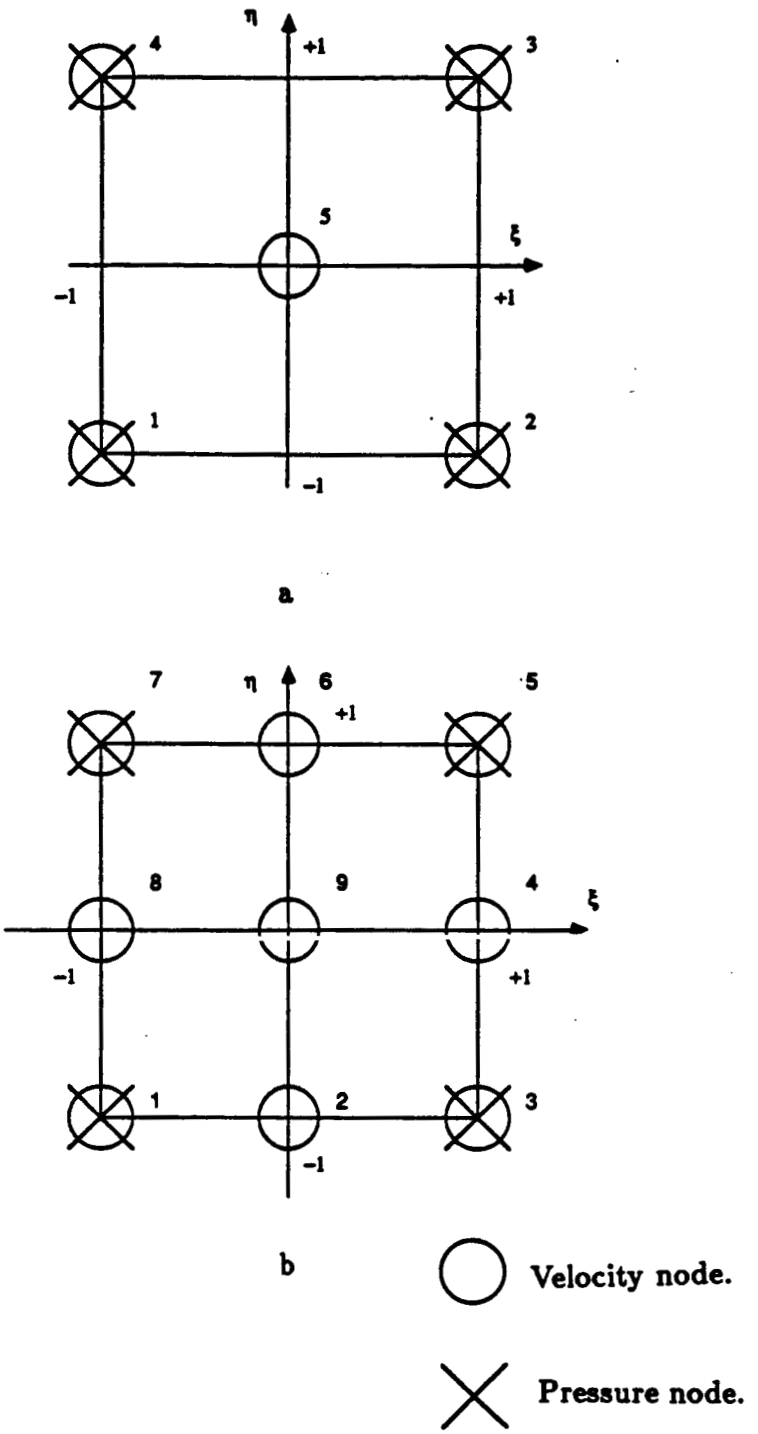

Figure 4.1. The four-node + bubble master element (a) and the nine-node master element (b).

associated with the equal order of interpolation.

The shape functions in the parent domain are (with the numbering of Figure 4.1) given below:

For velocity,

$$N_1 = \frac{1}{4}(1-\xi)(1-\eta) - \frac{1}{4}(1-\xi^2)(1-\eta^2) \tag{4.60}$$

$$N_2 = \frac{1}{4}(1+\xi)(1-\eta) - \frac{1}{4}(1-\xi^2)(1-\eta^2) \tag{4.61}$$

$$N_3 = \frac{1}{4}(1+\xi)(1+\eta) - \frac{1}{4}(1-\xi^2)(1-\eta^2) \tag{4.62}$$

$$N_4 = \frac{1}{4}(1-\xi)(1+\eta) - \frac{1}{4}(1-\xi^2)(1-\eta^2) \tag{4.63}$$

$$N_5 = (1-\xi^2)(1-\eta^2) \tag{4.64}$$

The interpolation of velocity is done through an incomplete second-order polynomial.

For pressure,

$$\hat{N}_1 = \frac{1}{4}(1-\xi)(1-\eta) \tag{4.65}$$

$$\hat{N}_2 = \frac{1}{4}(1+\xi)(1-\eta) \tag{4.66}$$

$$\hat{N}_3 = \frac{1}{4}(1+\xi)(1+\eta) \tag{4.67}$$

$$\hat{N}_4 = \frac{1}{4}(1-\xi)(1+\eta) \tag{4.68}$$

4.5.3 Existence of a checkerboard mode for the bubble-element

We will show that a checkerboard mode can exist when the mixed interpolation uses the bubble-element.

Consider a regular mesh of rectangular elements (Figure (4.2)). Using the local numbering of the nodes of element e, the pressure shape functions expressed in terms of the physical coordinates are

$$\hat{N}_1^e(x,y) = \frac{1}{h_i h_j}(x_{i+1}-x)(y_{j+1}-y) \tag{4.69}$$

$$\hat{N}_2^e(x,y) = \frac{1}{h_i h_j}(x-x_i)(y_{j+1}-y) \tag{4.70}$$

$$\hat{N}_3^e(x,y) = \frac{1}{h_i h_j}(x-x_i)(y-y_j) \tag{4.71}$$

$$\hat{N}_4^e(x,y) = \frac{1}{h_i h_j}(x_{i+1}-x)(y-y_j) \tag{4.72}$$

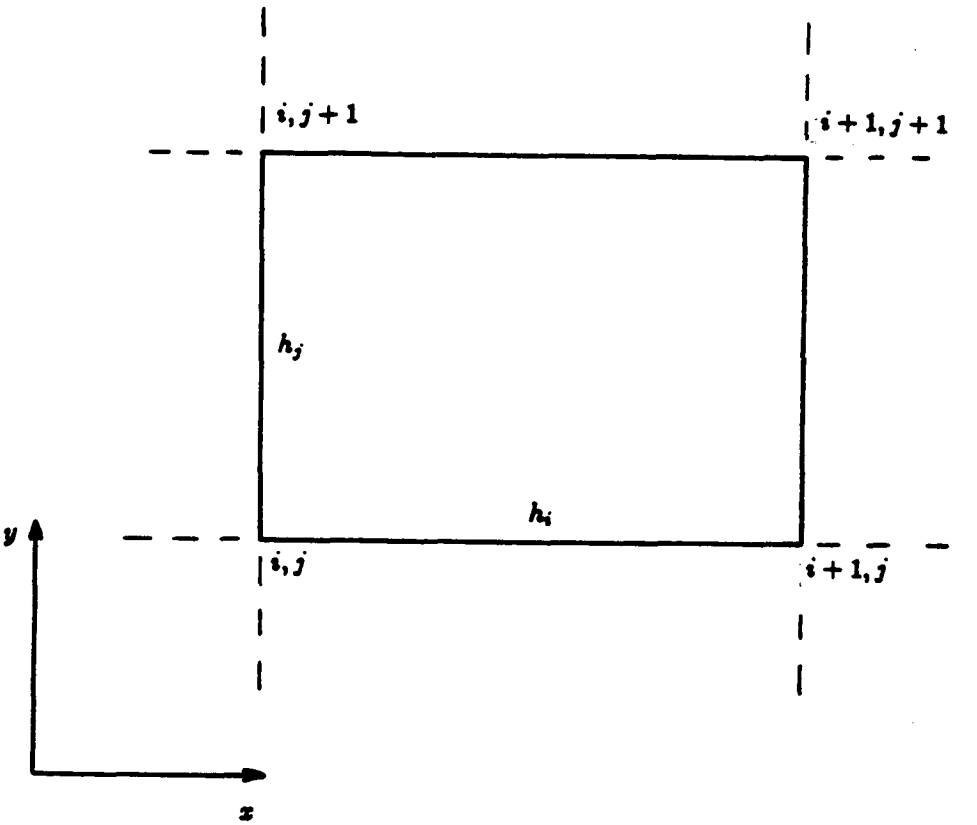

Figure 4.2. Global node numbering for a regular mesh.

The correspondance between the global coordinates (x, y) of a point M in the physical domain and the coordinates (ξ, η) of its image obtained by mapping the physical element into the parent (or master) element is given by

$$\begin{aligned} x(\xi,\eta) &= \sum_{a=1}^{4} \hat{N}_a(\xi,\eta) x_a \\ &= \frac{x_i + x_{i+1}}{2} + \frac{h_i}{2}\xi \end{aligned} \tag{4.73}$$

$$\begin{aligned} y(\xi,\eta) &= \sum_{a=1}^{4} \hat{N}_a(\xi,\eta) y_a \\ &= \frac{y_j + y_{j+1}}{2} + \frac{h_j}{2}\eta \end{aligned} \tag{4.74}$$

The element level discrete form of a checkerboard can be expressed as

$$p_a^e = p^e(M_a) = k(-1)^a \tag{4.75}$$

where M_a is a vertex of element e. Without loss of generality, we take $k = 1$. Using the expansion of p^e over the shape functions associated to element e, the interpolation of the spurious pressure mode is

$$\begin{aligned} p^e &= \sum_{a=1}^{4} \hat{N}_a p_a^e \\ &= -\hat{N}_1^e + \hat{N}_2^e - \hat{N}_3^e + \hat{N}_4^e \end{aligned} \tag{4.76}$$

Using the above relations, this becomes

$$p^e(\xi,\eta) = -\xi\eta \tag{4.77}$$

According to eqn (4.59), a discrete spurious pressure **p** mode can exist if it satisfies

$$\mathbf{Gp} = \mathbf{0}$$

The entry A_i of vector **Gp** is given by

$$\begin{aligned} \{\mathbf{Gp}\}_{A_i} &= \sum_{e=1}^{nel} \int_{\Omega^e} N_{a,i} \Big(\sum_{b=1}^{nenp} \hat{N}_b p_b^e \Big) d\Omega \\ &= \sum_{e=1}^{nel} \int_{-1}^{+1} \int_{-1}^{+1} (N_{a,\xi}\xi_{,i} + N_{a,\eta}\eta_{,i})(-\xi\eta) j \, d\xi d\eta \end{aligned} \tag{4.78}$$

where a is the local node number corresponding to A on element e, $nenp$ is the number of element nodal unknowns for the pressure, nel is the number of elements and j is the Jacobian determinant of the mapping from the physical domain into the parent domain.

We can express $N_{a,\xi}$ and $N_{a,\eta}$ as follows:
For $a = 1,2,3,4$,

$$N_{a,\xi} = \frac{1}{4}\xi_a(1+\eta_a\eta) + \frac{1}{2}\xi(1-\eta^2) \tag{4.79}$$

$$N_{a,\eta} = \frac{1}{4}\eta_a(1+\xi_a\xi) + \frac{1}{2}\eta(1-\xi^2) \tag{4.80}$$

For $a = 5$,

$$N_{5,\xi} = -2\xi(1-\eta^2) \tag{4.81}$$

$$N_{5,\eta} = -2\eta(1-\xi^2) \tag{4.82}$$

By substitution of eqns (4.79)-(4.80) into eqn (4.78), we obtain,
for $a = 1,2,3,4$,

$$\begin{aligned}
\{\mathbf{Gp}\}_{A_i} &= \sum_{e=1}^{nel}\int_{-1}^{+1}\int_{-1}^{+1}(\frac{1}{4}\xi_a(1+\eta_a\eta)+\frac{1}{2}\xi(1-\eta^2))(-\xi\eta)\xi_{,i}jd\xi d\eta \\
&+\sum_{e=1}^{nel}\int_{-1}^{+1}\int_{-1}^{+1}(\frac{1}{4}\eta_a(1+\xi_a\xi)+\frac{1}{2}\eta(1-\xi^2))(-\xi\eta)\eta_{,i}jd\xi d\eta \\
&=\sum_{e=1}^{nel}\int_{-1}^{+1}\int_{-1}^{+1}(-\frac{1}{4}\xi_a\xi\eta-\frac{1}{4}\xi_a\eta_a\xi\eta^2-\frac{1}{2}\xi^2\eta+\frac{1}{2}\xi^2\eta^3)\xi_{,i}jd\xi d\eta \\
&+\sum_{e=1}^{nel}\int_{-1}^{+1}\int_{-1}^{+1}(-\frac{1}{4}\eta_a\xi\eta-\frac{1}{4}\xi_a\eta_a\xi^2\eta-\frac{1}{2}\xi\eta^2+\frac{1}{2}\xi^3\eta^2)\eta_{,i}jd\xi d\eta
\end{aligned} \tag{4.83}$$

for $a = 5$,

$$\begin{aligned}
\{\mathbf{Gp}\}_{A_i} &= \sum_{e=1}^{nel}\int_{-1}^{+1}\int_{-1}^{+1}(-2\xi(1-\eta^2)(-\xi\eta))\xi_{,i}jd\xi d\eta \\
&+\sum_{e=1}^{nel}\int_{-1}^{+1}\int_{-1}^{+1}(-2\eta(1-\xi^2)(-\xi\eta)\eta_{,i}jd\xi d\eta \\
&=\sum_{e=1}^{nel}\int_{-1}^{+1}\int_{-1}^{+1}2(\xi^2\eta-\xi^2\eta^3)\xi_{,i}jd\xi d\eta \\
&+\sum_{e=1}^{nel}\int_{-1}^{+1}\int_{-1}^{+1}2(\xi\eta^2-\xi^3\eta^2)\eta_{,i}jd\xi d\eta
\end{aligned} \tag{4.84}$$

For a regular mesh of rectangular elements, $\xi_{,i}, \eta_{,i}$ and j are constant. Thus all the terms under the integral signs in eqns (4.83) and (4.84) contain odd powers of either ξ or η. Their integrals on the domain centered on $(0,0)$ are equal to zero. This means that the checkerboard pressure mode satisfies the equation

$$\mathbf{Gp} = \mathbf{0}$$

4.5.4 Treatment of the spurious pressure mode

The correct pressure field can be recovered through a filtering technique [18]. In the presence of a checkerboard pressure mode, the computed pressure field can be written

$$\hat{p} = p + p_c \tag{4.85}$$

where p is the correct pressure field and p_c is the checkerboard pressure. For a regular mesh of rectangular element, the interpolation of the checkerboard pressure over one element is

$$p_c^e(M_a) = (-1)^a k \tag{4.86}$$

where M_a is a vertex of the pressure discretization, and k is an arbitrary constant.

To filter the pressure solution and recover an acceptable pressure field, we use the following two-step approach:

First step: Averaging.

The pressure $\hat{p}$ is averaged over each element through

$$\bar{p}^e(\Omega^e) = \frac{1}{4}\sum_{a=1}^{4}\hat{p}_a \tag{4.87}$$

where $\hat{p}_a$ is the value of the pressure at node a of element e. In the case of a regular mesh of rectangular elements, we have

$$\bar{p}^e(\Omega^e) = \frac{1}{4}\sum_{a=1}^{4} p(M_a), \tag{4.88}$$

that is , the averaging removes the checkerboard.

Second step: Least-squares approximation.

We recover the nodal values of the pressure through a least-squares approach. Let p denote the unknown discrete pressure field, and let $\bar{p}$ denote the discrete averaged pressure field. Let $J(p)$ be the functional

$$J(p) = \int_\Omega (\bar{p} - p)^2 d\Omega \tag{4.89}$$

Let us expand p over the basis of the pressure approximation as

$$p = \sum_{B=1}^{np} p_B \hat{N}_B \tag{4.90}$$

where np is the number of unknown nodal pressure values. Then $J(p)$ can be written

$$J(p) = \int_\Omega (\bar{p} - \sum_{B=1}^{np} p_B \hat{N}_B)^2 d\Omega \tag{4.91}$$

We look for p such that $J(p)$ is a minimum,i.e.,

$$\delta J = 0 \tag{4.92}$$

But

$$\delta J = 0 \Rightarrow \frac{\partial J}{\partial p_C} = 0 \qquad \forall C = 1, ..., np \tag{4.93}$$

Now

$$\frac{\partial J}{\partial p_C} = -2 \int_\Omega (\bar{p} - \sum_{B=1}^{np} p_B \hat{N}_B) \hat{N}_C d\Omega \tag{4.94}$$

and

$$\frac{\partial J}{\partial p_C} = 0 \Rightarrow \int_\Omega \bar{p} \hat{N}_C d\Omega = \int_\Omega (\sum_{B=1}^{np} p_B \hat{N}_B) \hat{N}_C d\Omega \qquad \forall C = 1, ..., np \tag{4.95}$$

or equivalently

$$(\sum_{B=1}^{np} \int_\Omega \hat{N}_B \hat{N}_C d\Omega) p_B = \int_\Omega \bar{p} \hat{N}_C d\Omega \quad \forall C = 1, ...np \tag{4.96}$$

Let $\mathbf{p}$ be the vector of unknown nodal values of p. Then the above equation system can be written as

$$\mathbf{Mp} = \mathbf{F} \tag{4.97}$$

where

$$\mathbf{M}_{CB} = \{\int_\Omega \hat{N}_B \hat{N}_C d\Omega\} \tag{4.98}$$

and

$$\mathbf{F}_C = \int_\Omega \bar{p} \hat{N}_C d\Omega \tag{4.99}$$

The matrix $\mathbf{M}$ has the structure of a mass matrix arising from a finite element discretization.

Remark:

In eqn (4.75), the form of the checkerboard could be expressed more generally as

$$p_a^e = k_1(-1)^a + k_2 \tag{4.100}$$

where k_2 is an arbitrary constant. A constant pressure field satisfying eqn (4.59) is called an hydrostatic pressure mode. For any contained flow, the pressure is known up to an arbitrary constant and the hydrostatic pressure mode exists. The usual cure to that problem is to specify the pressure at one node. However in that case the constants k_1 and k_2 adjust so that the constraint is satisfied. But the checkerboard is not removed. In the treatment of the pressure mode, the averaging step only removes the nonconstant part of the checkerboard, and the final smoothed pressure is known up to a constant.

It has been pointed out [18,19] that a method of the type described previously does not give good results at the boundaries and/or corners of the domain. More sophisticated algorithm including extrapolation procedures or special treatments at the boundary and corner nodes are described in [18,19].

4.5.5 The nine-node Lagrange element

This element is standard for the mixed finite-element method using a quadratic velocity/bilinear pressure interpolation. It has been extensively used and its good properties have been long established [6,17].

This element contains 9 velocity nodes and 4 pressure nodes (Figure 4.1). The shape functions in the parent domain are given below:

For velocity,

$$N_1 = \frac{1}{4}(1-\xi)(1-\eta)\xi\eta \tag{4.101}$$

$$N_2 = -\frac{1}{2}(1-\xi^2)(1-\eta)\eta \tag{4.102}$$

$$N_3 = -\frac{1}{4}(1+\xi)(1-\eta)\xi\eta \tag{4.103}$$

$$N_4 = \frac{1}{2}(1+\xi)(1-\eta^2)\xi \tag{4.104}$$

$$N_5 = \frac{1}{4}(1+\xi)(1+\eta)\xi\eta \tag{4.105}$$

$$N_6 = \frac{1}{2}(1-\xi^2)(1+\eta)\eta \tag{4.106}$$

$$N_7 = -\frac{1}{4}(1-\xi)(1+\eta)\xi\eta \tag{4.107}$$

$$N_8 = -\frac{1}{2}(1-\xi)(1-\eta^2)\xi \tag{4.108}$$

$$N_9 = (1-\xi^2)(1-\eta^2) \tag{4.109}$$

The interpolation functions for the pressure are the same as for the four-node + bubble element (see eqn (4.65)-(4.68)).

CHAPTER 5: NUMERICAL EXAMPLES

5.1 Lid-driven cavity flow

The lid-driven cavity flow is a typical example of internal flow. The simplicity of the geometry makes it one of the favored test problems in computational fluid dynamics.

The motion of the upper wall of the cavity induces the development of the flow field. The flow being contained, viscous stresses are solely responsible for the initial motion of the fluid. However for high Reynolds numbers, the convective effects become significant and dominant for the development of the flow patterns,in particular for the occurence of recirculation regions at the bottom corners of the cavity.

The Reynolds number is defined as

$$Re = \frac{U_w D}{\nu} \tag{5.1}$$

where U_w is the tangential velocity of the upper wall, D is the size of the square cavity and ν is the kinematic viscosity of the fluid.

The domain and boundary conditions for both the primitive variable and the vorticity stream-function formulations are given in Figure 5.1. For the velocity-pressure formulation, the four-node + bubble element and the nine-node Lagrange element have been tested. For the later case as well as for the vorticity stream-function formulation, the meshes have 32×32 square elements, whereas a mesh of 20×20 square elements has been used for the four-node + bubble element. Moreover in the case of the four-node + bubble element, a Galerkin formulation was employed.

For the velocity-pressure formulation, the boundaries are of pure Dirichlet type and are easy to implement. A pressure data is given at a point on the boundary to set the hydrostatic pressure level. For the vorticity stream-function formulation there are no boundary conditions for vorticity (because all the boundaries are walls). The stream function is constant all over the boundaries, and its normal derivative is zero for the left, bottom and right walls and is equal to the lid velocity at the upper boundary. In the vorticity stream-function formulation as well as the velocity- pressure formulation, the boundary conditions at the upper corners are discontinuous. However, this has produced no problem throughout the computations.

The Reynolds numbers investigated in this study are 400 (Figure 5.2) and 1000 (Figure 5.3) for the vorticity stream-function formulation and 400 (Figures 5.4 and 5.5) for the velocity-pressure formulation.

For this range of Reynolds numbers , the main structures of the flow are the primary vortex and the two secondary vortices. The primary vortex is created in the upper right region. As it grows, its center moves down toward the center of the cavity. The two secondary vortices develop at the lower left and right corners.

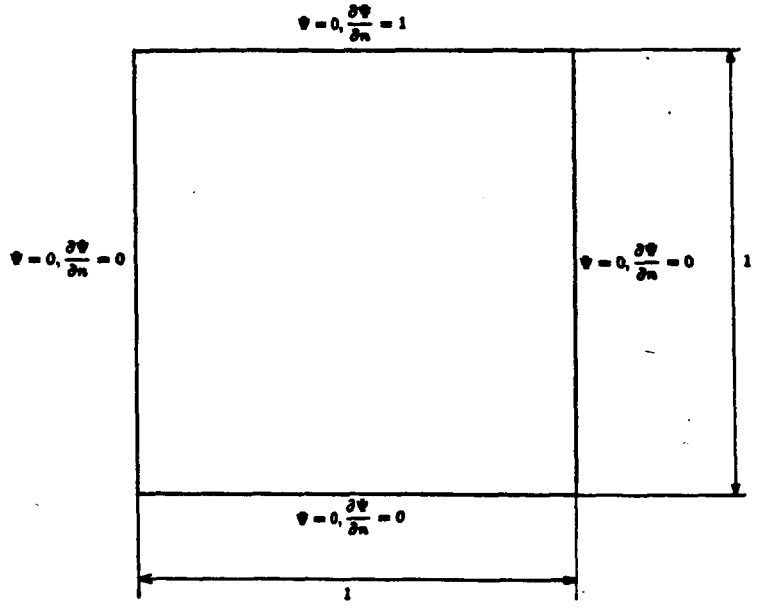

a

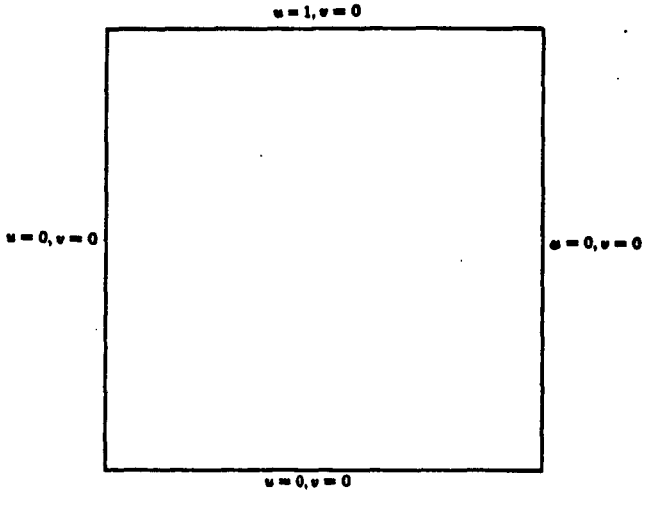

b

Figure 5.1. Lid-driven cavity flow : Problem domain and boundary conditions for the vorticity stream-function formulation (a) and the velocity-pressure formulation (b).

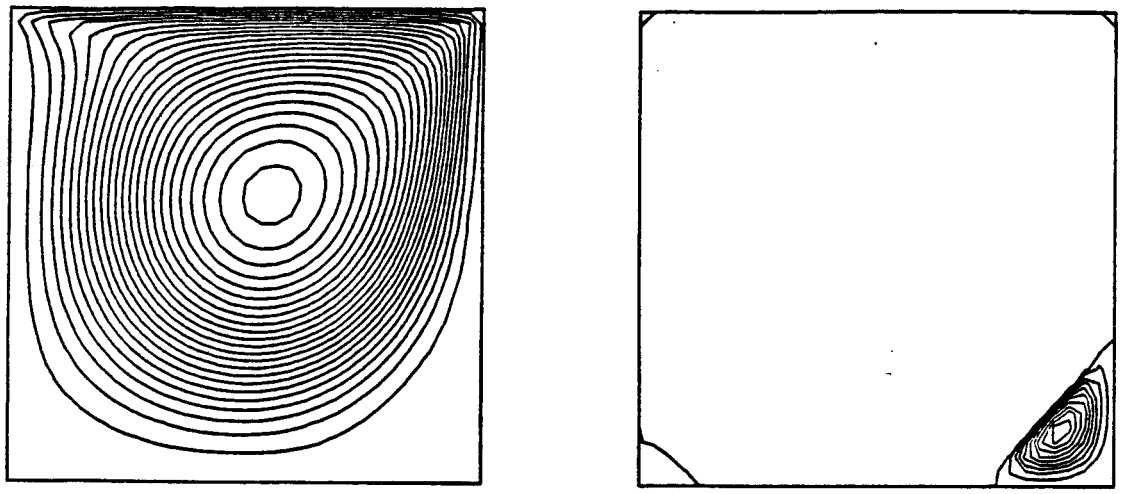

a b

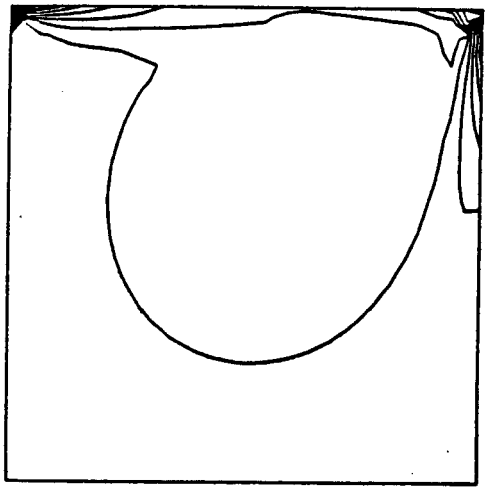

c

Figure 5.2. Lid-driven cavity flow: Steady-state solutions obtained by the vorticity stream-function formulation at Re=400; a) Streamlines; b) Corner streamlines; c) Vorticity.

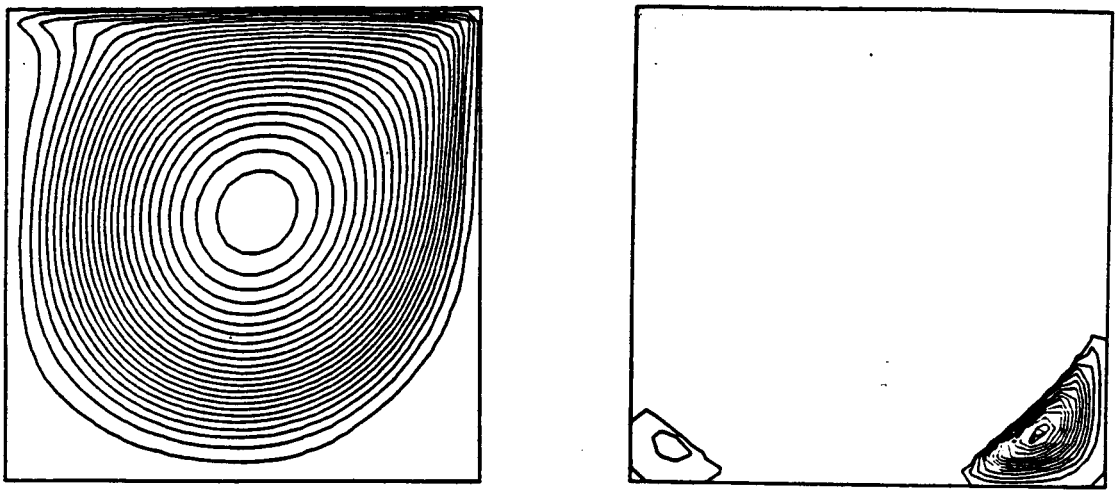

a b

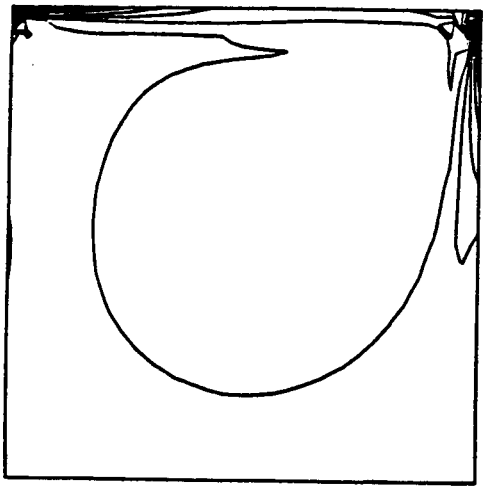

c

Figure 5.3. Lid-driven cavity flow: Steady-state solutions obtained by the vorticity stream-function formulation at Re=1000; a) Streamlines; b) Corner streamlines; c) Vorticity.

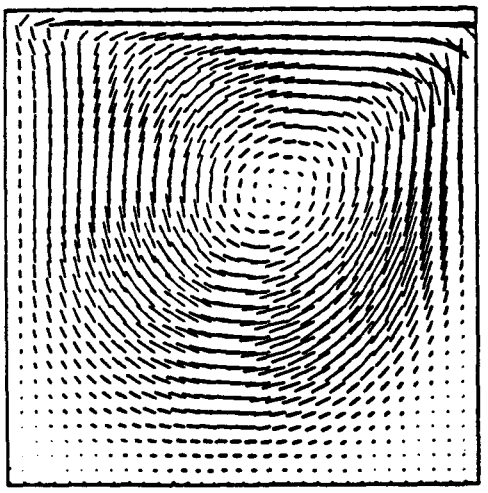

a

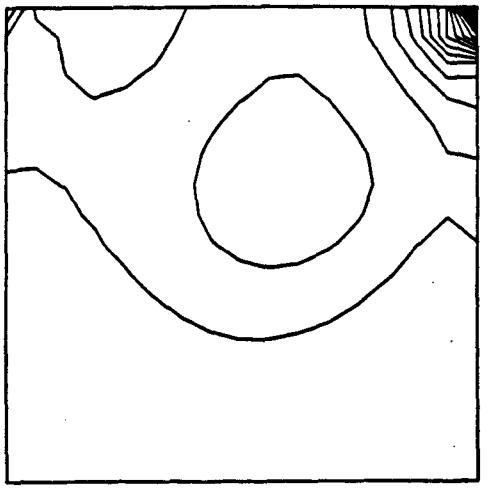

b

Figure 5.4. Lid-driven cavity flow: Steady-state solutions obtained by the velocity-pressure formulation using the nine-node element, at Re=400; a) Velocity; b) Pressure.

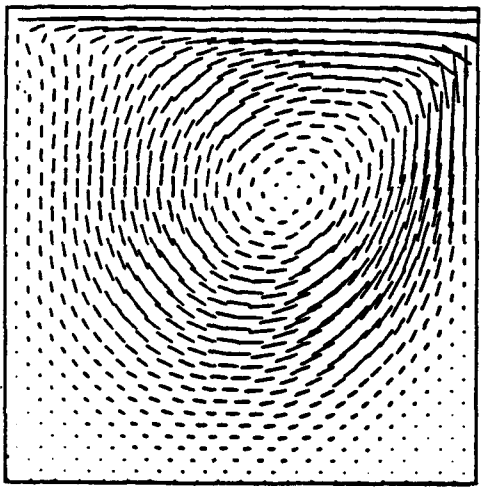

a

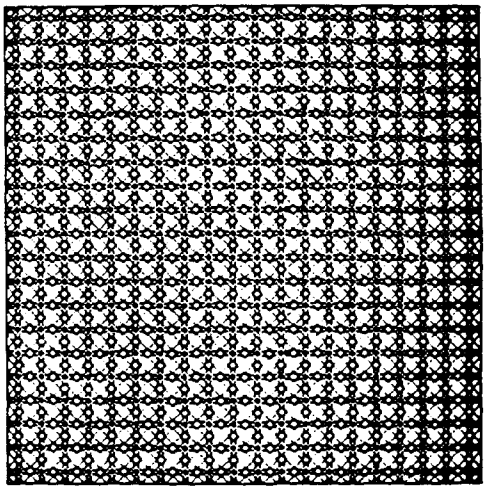

b

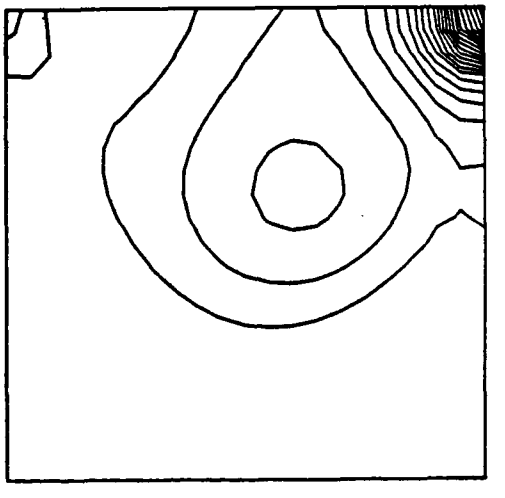

c

Figure 5.5. Lid-driven cavity flow: Steady-state solutions obtained by the velocity pressure formulation using the four-node + bubble element, at Re=400; a) Velocity; b) Nonsmoothened pressure; c) Smoothened pressure.

For moderate Reynolds numbers, the span of the vortex at the lower right corner of the cavity is larger than that at the lower left corner.

The results obtained for both formulations are in good agreement with available data [19]. For a Reynolds number of 400, in both cases, the coordinates of the center of the primary vortex agree with the data given in [19] with a precision better than the node-to-node distance of the mesh.

In the case of the four-node + bubble element, the pathology described in Section 5.4.3 , i.e, a pressure field polluted by a checkerboard mode, has been observed. The polluted pressure field has been treated through the procedure advocated in Section 5.4.4 to recover an acceptable pressure distribution. The results are shown in Figure 5.5.

5.2 Plane jet flow

This case has been studied only with the vorticity stream-function formulation. The problem domain and the boundary conditions are depicted in Figure 5.6. The finite-element mesh has 64×64 square elements. For that problem, the Reynolds number is defined as

$$Re = \frac{a\bar{U}}{\nu} \tag{5.2}$$

where a is the width of the jet aperture, $\bar{U}$ is the mean velocity at the inlet and ν is the kinematic viscosity of the fluid. The inlet velocity profile is parabolic and the Reynolds number is 167. The motivation for that simulation was to study the development of a plane jet in an open domain and our goal was to show the capability of our numerical scheme to simulate the breaking of symmetry in an initially symmetrical flow.

In the initial state, the fluid is at rest. When the jet develops, the shearing effect between the front of fast moving fluid and the surrounding resting fluid induces the formation of two symmetrical vortices (Figure 5.7). The vortices grow as they move toward the right (downstream) boundary of the domain (Figures 5.8 and 5.9).

The selection of the boundary conditions for that case is important. The condition,

$$\frac{\partial \Psi}{\partial n} = 0 \tag{5.3}$$

which is applied on upper, lower and right (downstream) boundaries, implies

$$u_\tau = 0 \tag{5.4}$$

The effect of these boundary conditions on the flow field is especially seen in Figure 5.9, where the streamlines at the downstream boundary curve and cross the limit of the domain at right angle.

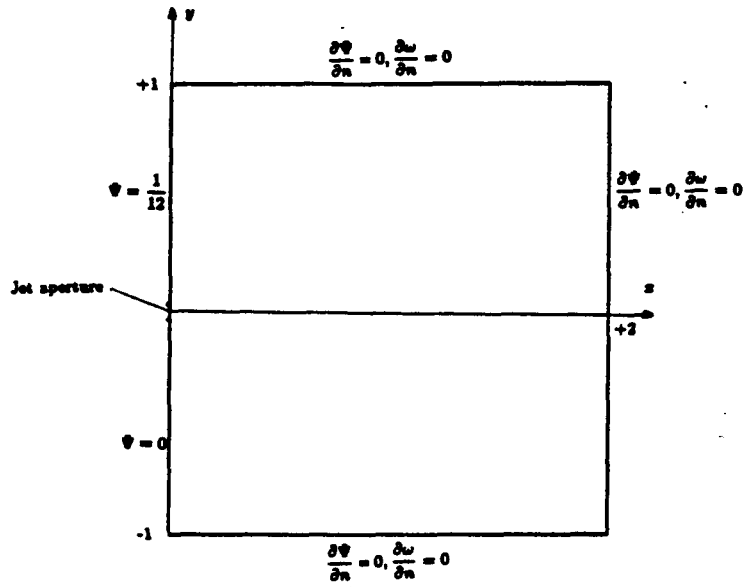

a

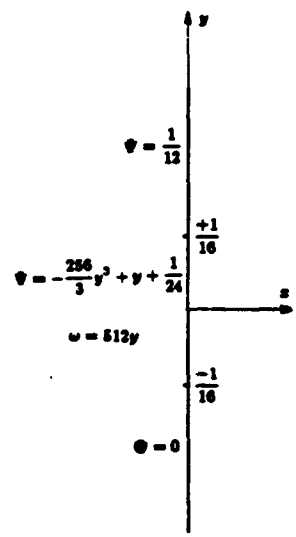

b

Figure 5.6. Plane jet flow: Problem domain and boundary conditions for the vorticity stream-function formulation; a) Whole domain; b) Close view of the jet aperture.

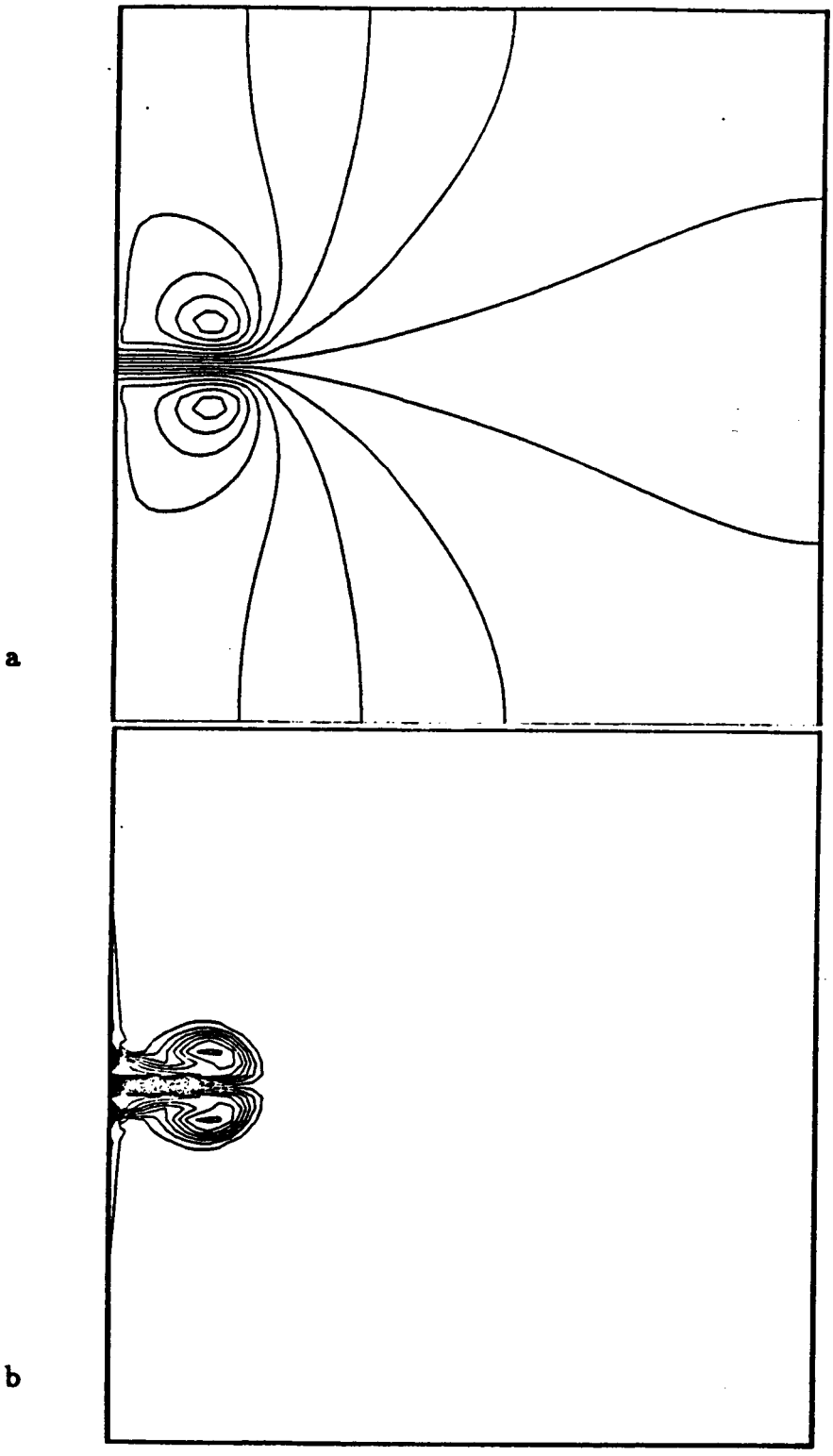

Figure 5.7. Plane jet flow: Solution obtained by the vorticity stream-function formulation at t=1.2s; a) Streamlines; b) Vorticity.

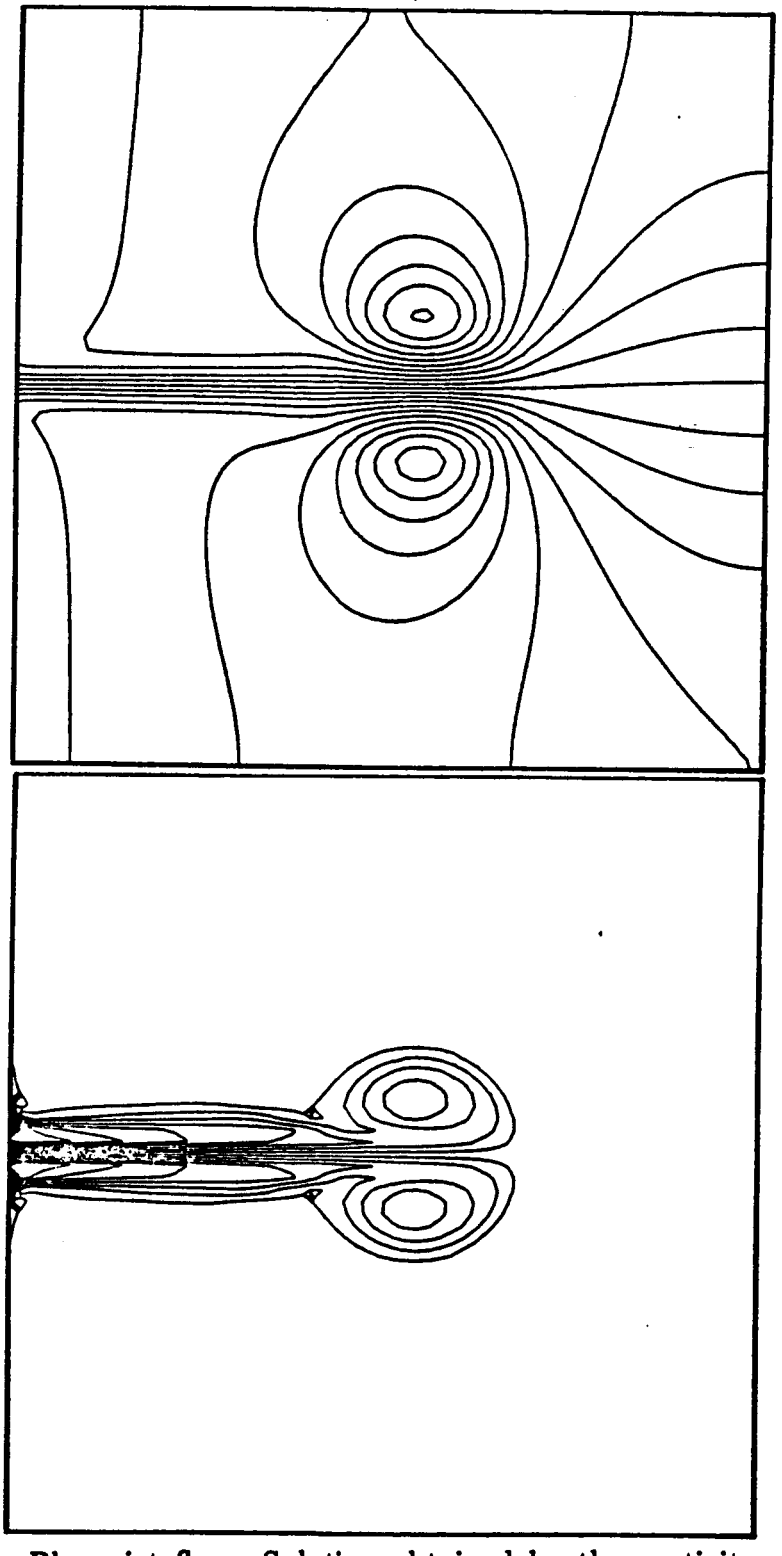

Figure 5.8. Plane jet flow: Solution obtained by the vorticity stream-function formulation at t=3.6s; a) Streamlines; b) Vorticity.

a

b

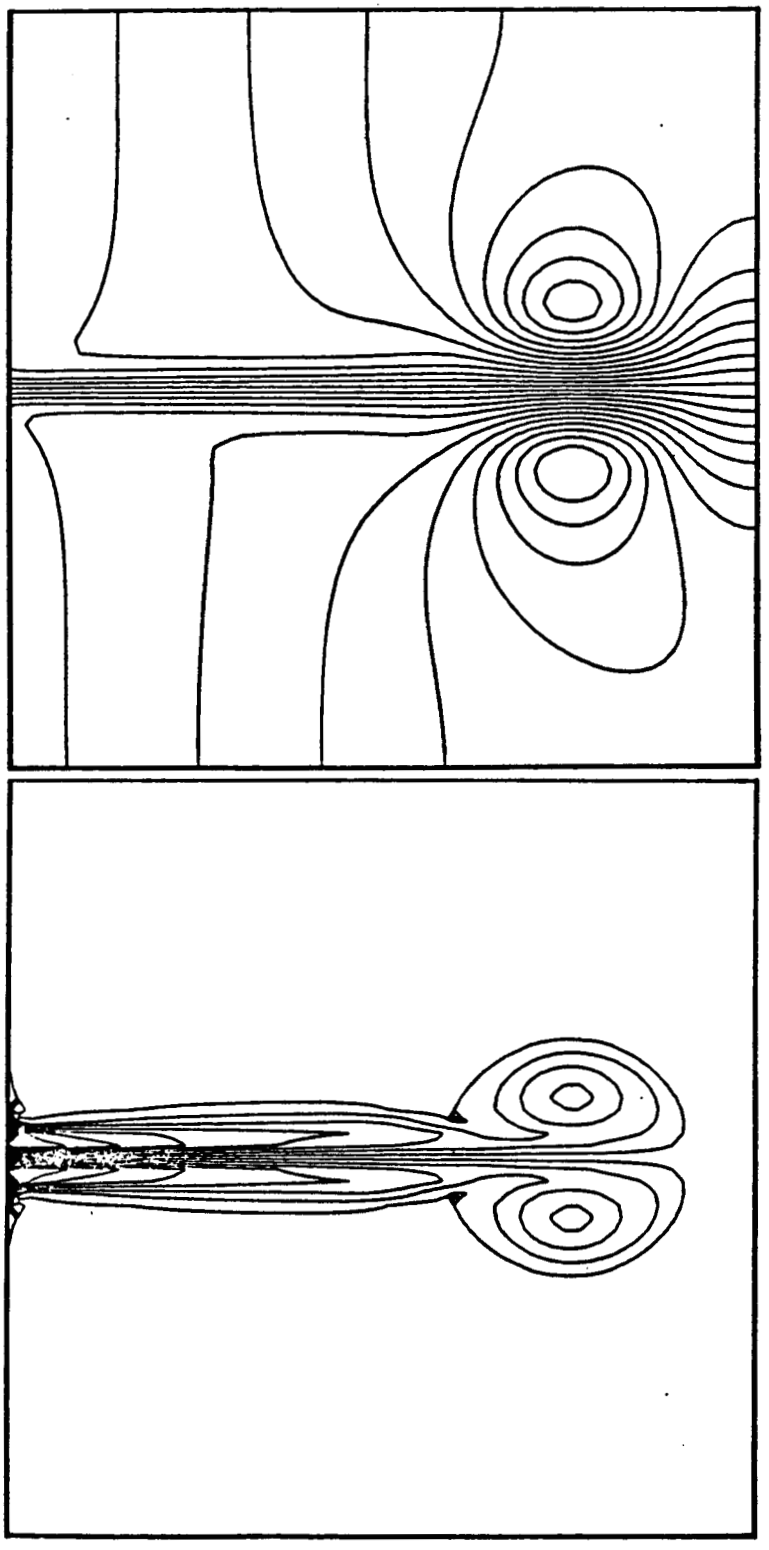

Figure 5.9. Plane jet flow: Solution obtained by the vorticity stream-function formulation at t=4.8s; a) Streamlines; b) Vorticity.

After the two vortices associated with the early development of the flow have left the computational domain, a steady-state symmetrical flow is obtained (Figure 5.10).

This flow is perturbed by modifying the inlet velocity profile over one time step. This is obtained by adding a 3% perturbation to the nodal values of the vorticity in the lower half of the inlet. The perturbed flow develops then in a nonsymmetrical pattern. Vortices form and pair as they are carried downstream (Figures 5.11 to 5.13).

The amount of perturbation added to disturb the flow should not influence the final flow field. Bristeau et al. [1] have reported results using a Galerkin formulation with a very fine unsymmetrical mesh. Their solution shows the breaking of symmetry without adding a perturbation. The use of a nonsymmetrical mesh acts as a perturbation that triggers the development of a nonsymmetrical solution.

5.3 Flow past a circular cylinder

The flow of a viscous fluid past a circular cylinder is one of the most extensively studied cases and has become a classical test for numerical procedures [5,8]. It is of engineering interest because it presents most of the flow features that are encountered in more complicated external flow situations such as separation and vortex shedding [20,21]. In fact the cylinder can be seen as the basic shape that can be degenerated in all the more complicated symmetrical and nonsymmetrical profiles. This case has been investigated using both the primitive variable and the vorticity stream-function formulations. In both cases, symmetrical flow solutions are first obtained and then perturbed to produce vortex shedding in the wake of the cylinder.

The meshes and boundary conditions for the two formulations are shown in Figures 5.14 and 5.15. For the velocity-pressure formulation, only the nine-node Lagrange elements were used.

For this flow, the Reynolds number is defined as

$$Re = \frac{U_\infty d}{\nu} \tag{5.5}$$

where U_∞ is the inlet velocity, d is the diameter of the cylinder, and ν is the kinematic viscosity of the fluid. The present study has been carried out for $Re = 100$.

The specified inlet velocity profile is a constant. For the upper and lower boundaries, in the velocity-pressure formulation, we specify zero tangential stress and zero vertical velocity whereas in the vorticity stream-function formulation, the value of the stream function is specified and the vorticity is set to zero. From a physical point of view, these boundary conditions are equivalent. However they are only valid if the boundaries are far enough from the cylinder so that the vorticity generated in the boundary layer at the cylinder surface does not diffuse up to the outer boundaries. In a finite-difference framework, the boundaries of the domain

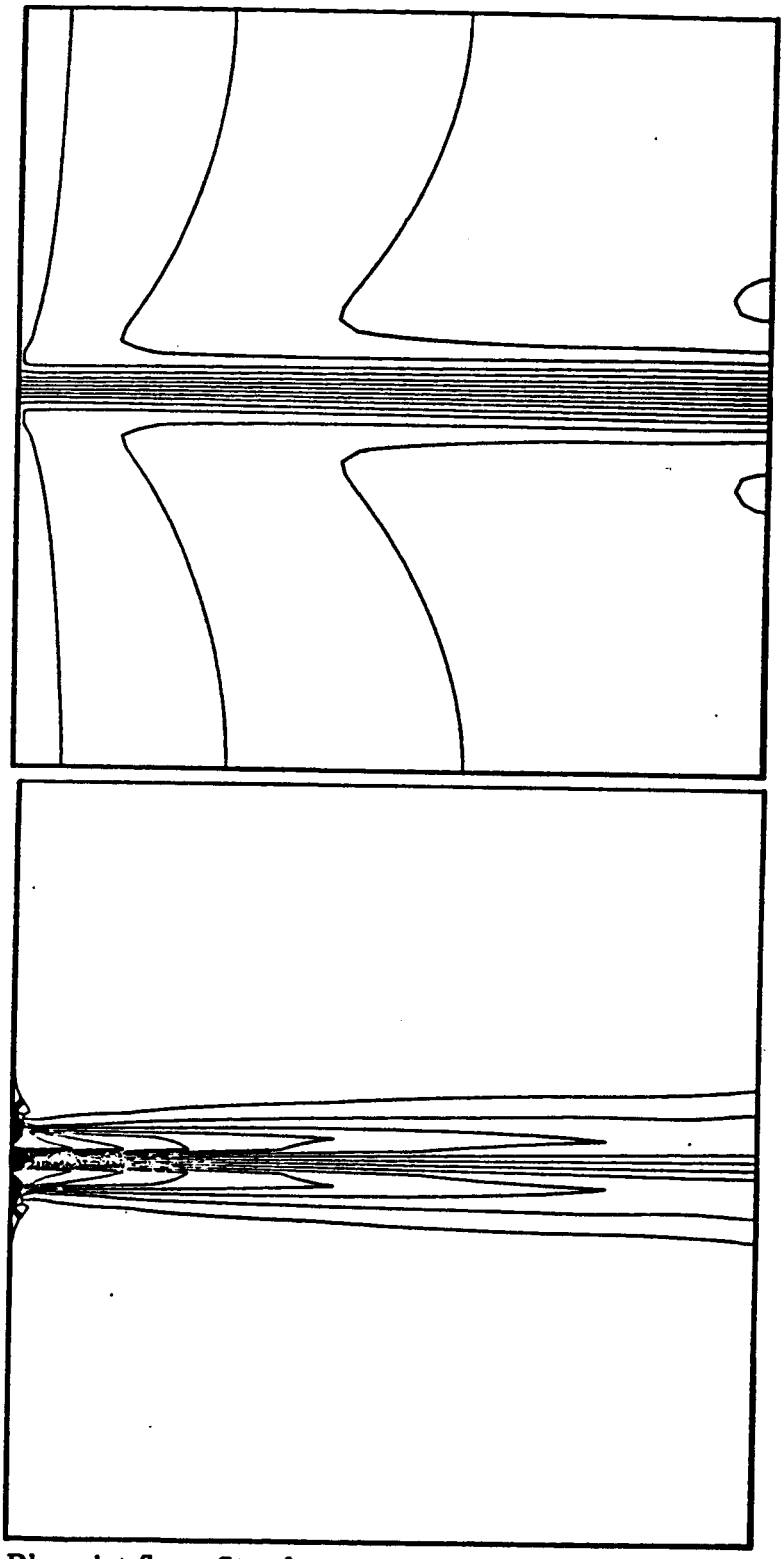

Figure 5.10. Plane jet flow: Steady-state solution obtained by the vorticity stream-function formulation; a) Streamlines; b) Vorticity.

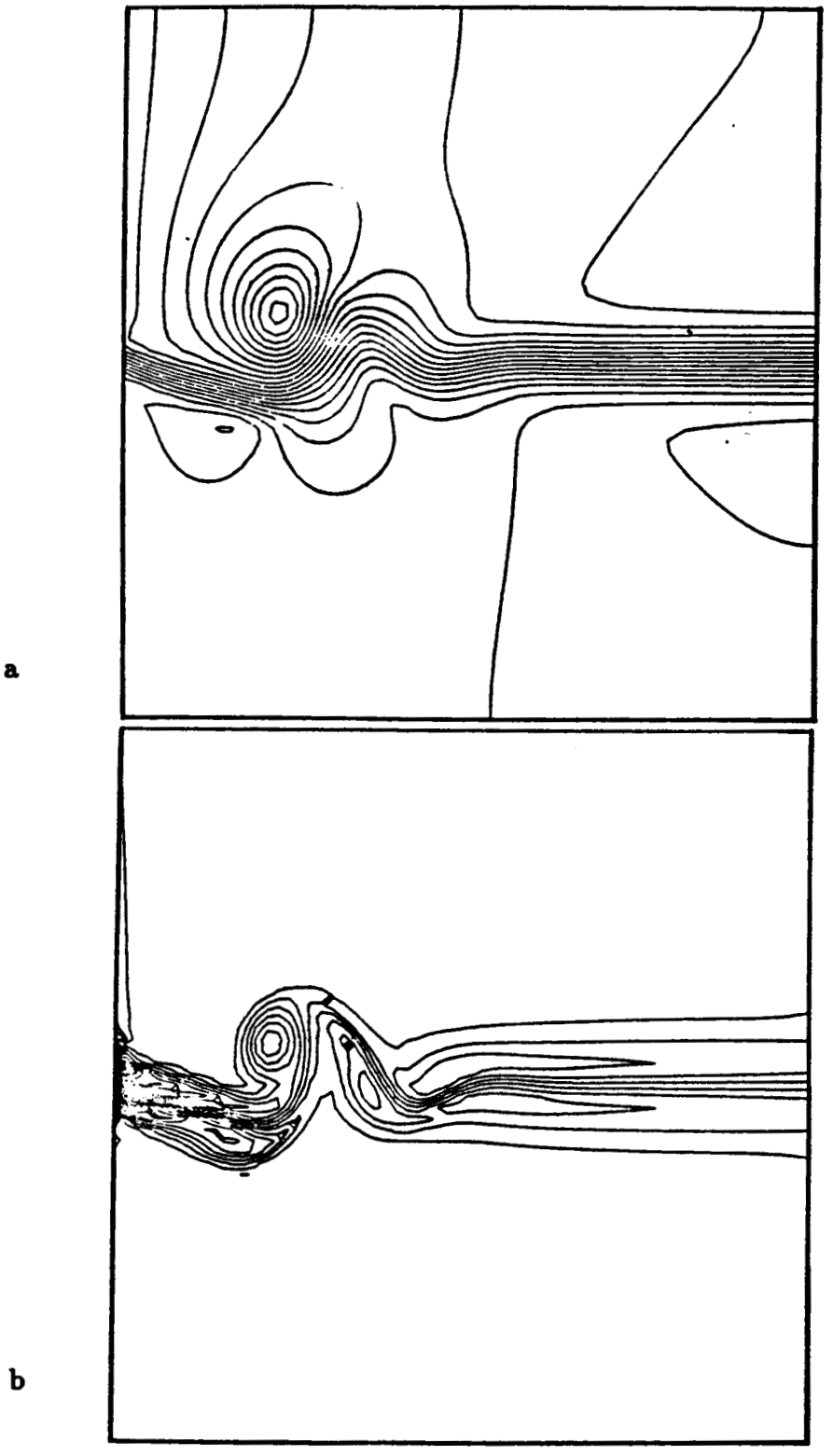

Figure 5.11. Plane jet flow: Solution obtained by the vorticity stream-function formulation at t=1.2s after perturbation; a) Streamlines; b) Vorticity.

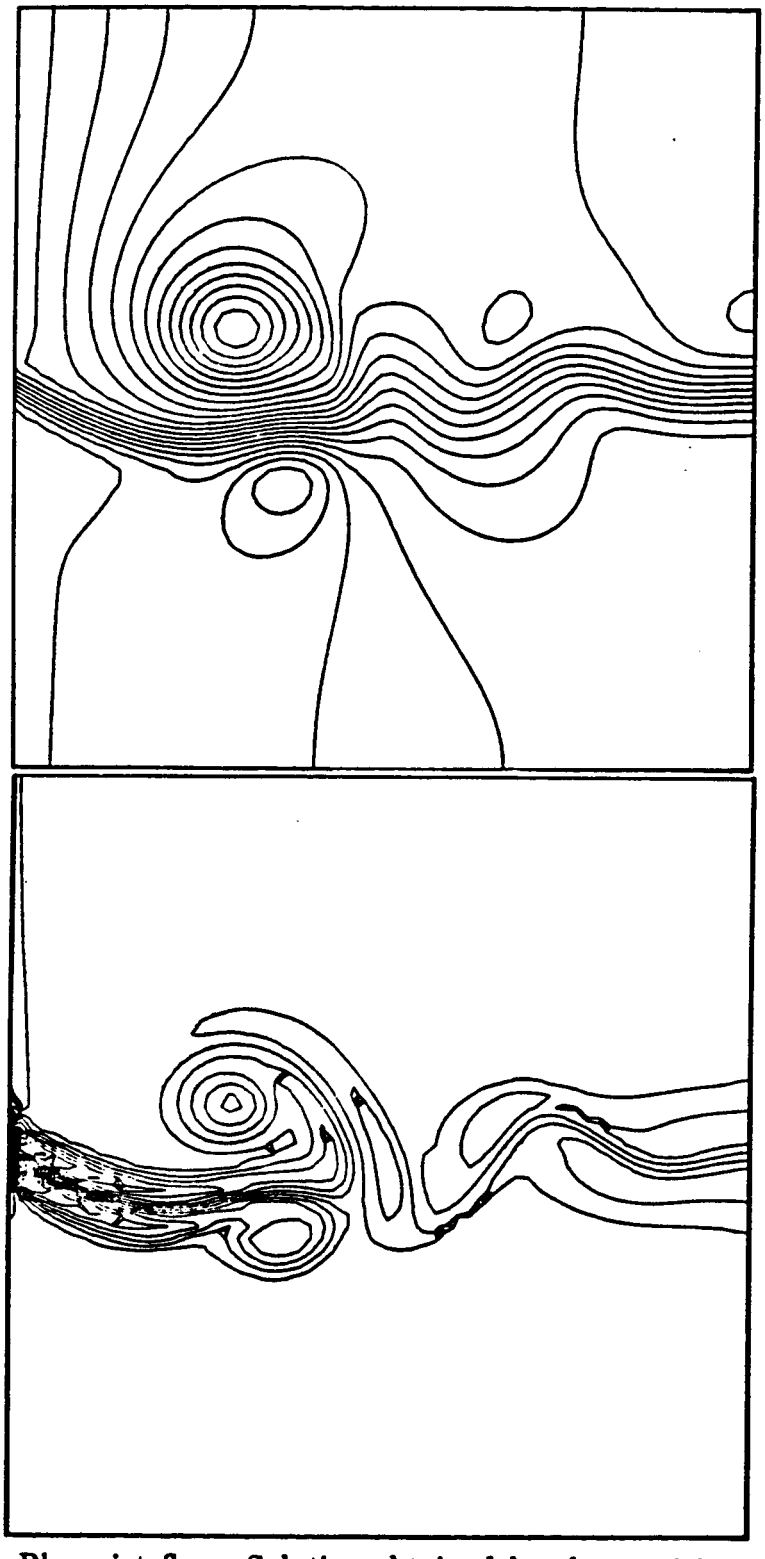

Figure 5.12. Plane jet flow: Solution obtained by the vorticity stream-function formulation at t=2.4s after perturbation; a) Streamlines; b) Vorticity.

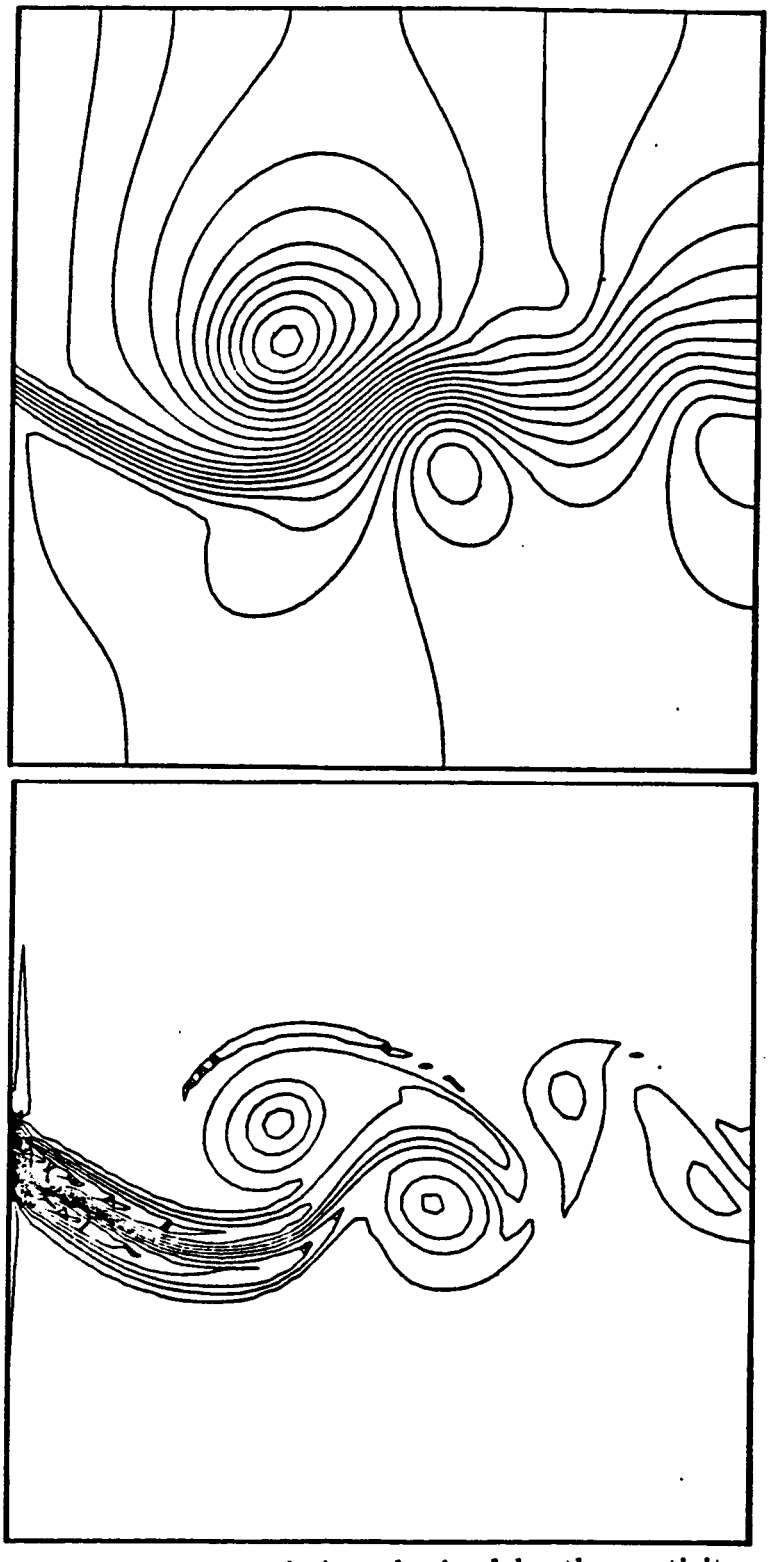

Figure 5.13. Plane jet flow: Solution obtained by the vorticity stream-function formulation at t=3.6s after perturbation; a) Streamlines; b) Vorticity.

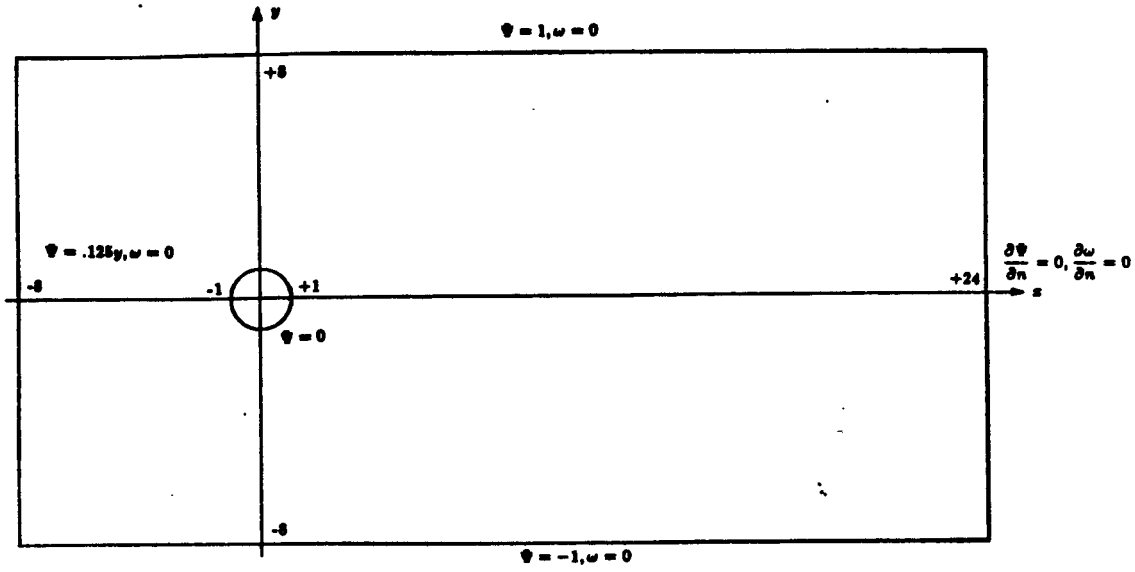

a

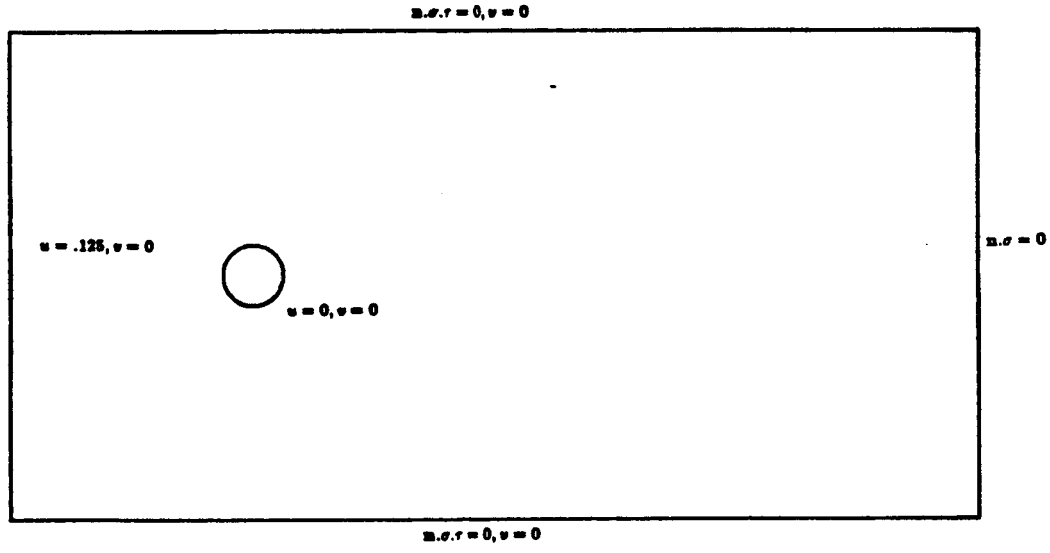

b

Figure 5.14. Flow past a circular cylinder: Problem domain and boundary conditions for the vorticity stream-function formulation (a) and the velocity-pressure formulation (b).

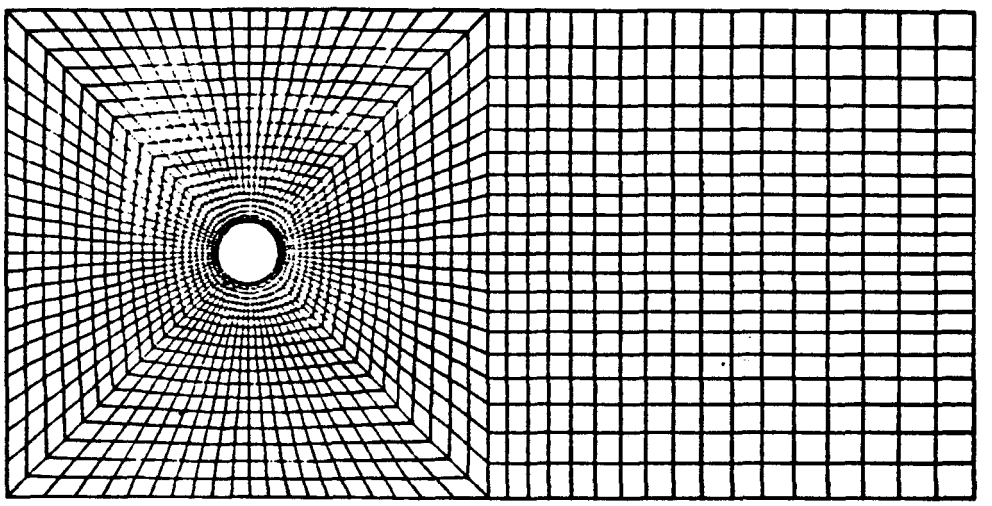

a

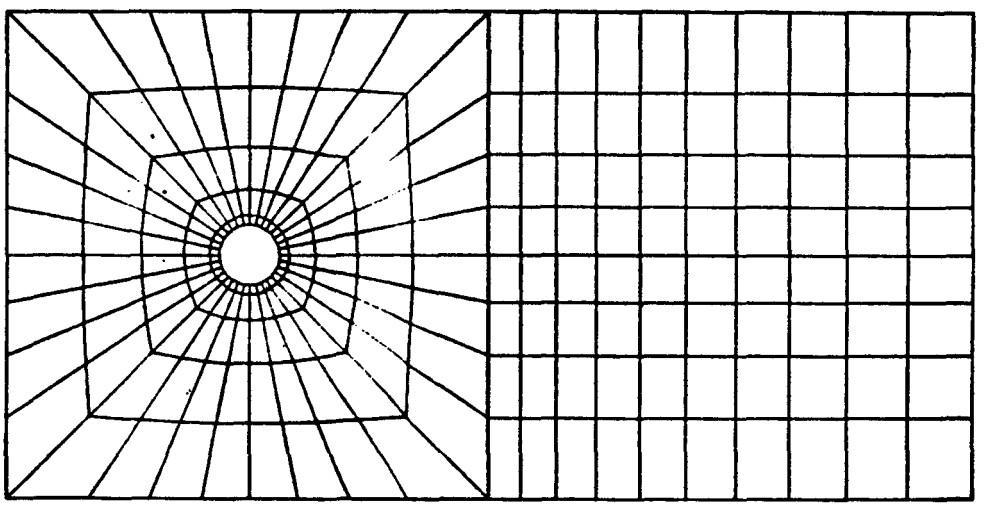

b

Figure 5.15. Flow past a circular cylinder: Finite-element meshes for the vorticity stream-function formulation (a) and the velocity-pressure formulation (b).

can be set at an arbitrary large distance from the cylinder through mapping techniques. In the finite-element method, procedures such as exponential stretching are used to render the infinity of the computational domain. In the present study, following the work of Gresho [5] and Hughes [7], we used a domain of finite extent. This presumably induced a blockage effect in the flow around the cylinder [7], but did not prevent us from simulating the main flow features such as the recirculation and the vortex shedding. At the downstream boundary, the stress is set to zero in both tangential and normal directions in the primitive variable formulation and the normal derivatives of vorticity and stream function are set to zero in the vorticity stream-function formulation. Those boundary conditions are not equivalent. Setting the stress to zero imposes no constraint on the direction of the flow at the boundary whereas a zero normal derivative of the stream function forces the streamlines to leave the domain in a direction normal to the boundary. However, this effect is of small influence on the computed flow. At the cylinder surface, the boundary conditions are naturally the no-slip conditions which are staightforward in the velocity-pressure formulation. For the vorticity stream-function equations, as explained earlier, there are no obvious boundary conditions at a solid surface. In the present case, we take advantage of the symmetry of the domain to set the value of the stream function at the cylinder. When the nonsymmetrical flow is studied, this condition is no more valid. In fact because the stream function is set at the upper and lower boundaries and at the cylinder surface, the flow rate is constrained to be the same above and under the cylinder. The previous remarks show that for external flows, the boundary conditions of the primitive variable formulation are more accurate and easier to implement than those of the vorticity stream-function formulation.

For both cases, the flow develops in a symmetrical pattern (Figures 5.16 and 5.17). Two standing vortices grow in the wake of the cylinder. In experimental studies [22] of such a flow, nonsymmetrical solutions presenting vortex shedding have been observed for Reynolds number greater than 40. Symmetrical solutions can not be obtained experimentally because the flow is unstable for any perturbation, and of course, in an experimental set up perturbations cannot be avoided. This is not the case for a numerical study. The mesh we have used is symmetrical and all the conditions are symmetrical up to the last digits. The computations being performed in double precision, the level of unsymmetry is virtually reduced to zero.

The nonsymmetrical flow is obtained by perturbing the steady symmetrical solution. In the case of the vorticity stream-function formulation, this is done by introducing some artificial vorticity at the centerline in the near wake of the cylinder before restarting the computations. The perturbation amounts to 5% of the maximum value of the vorticity in the flow field. For the primitive variable formulation, the cylinder is rotated in the counterclockwise direction over four time steps. It would be simpler to perturb the velocity field at the centerline in the wake of the cylinder, but this would produce a nonsolenoidal flow field which could lead to nonconverging computations.

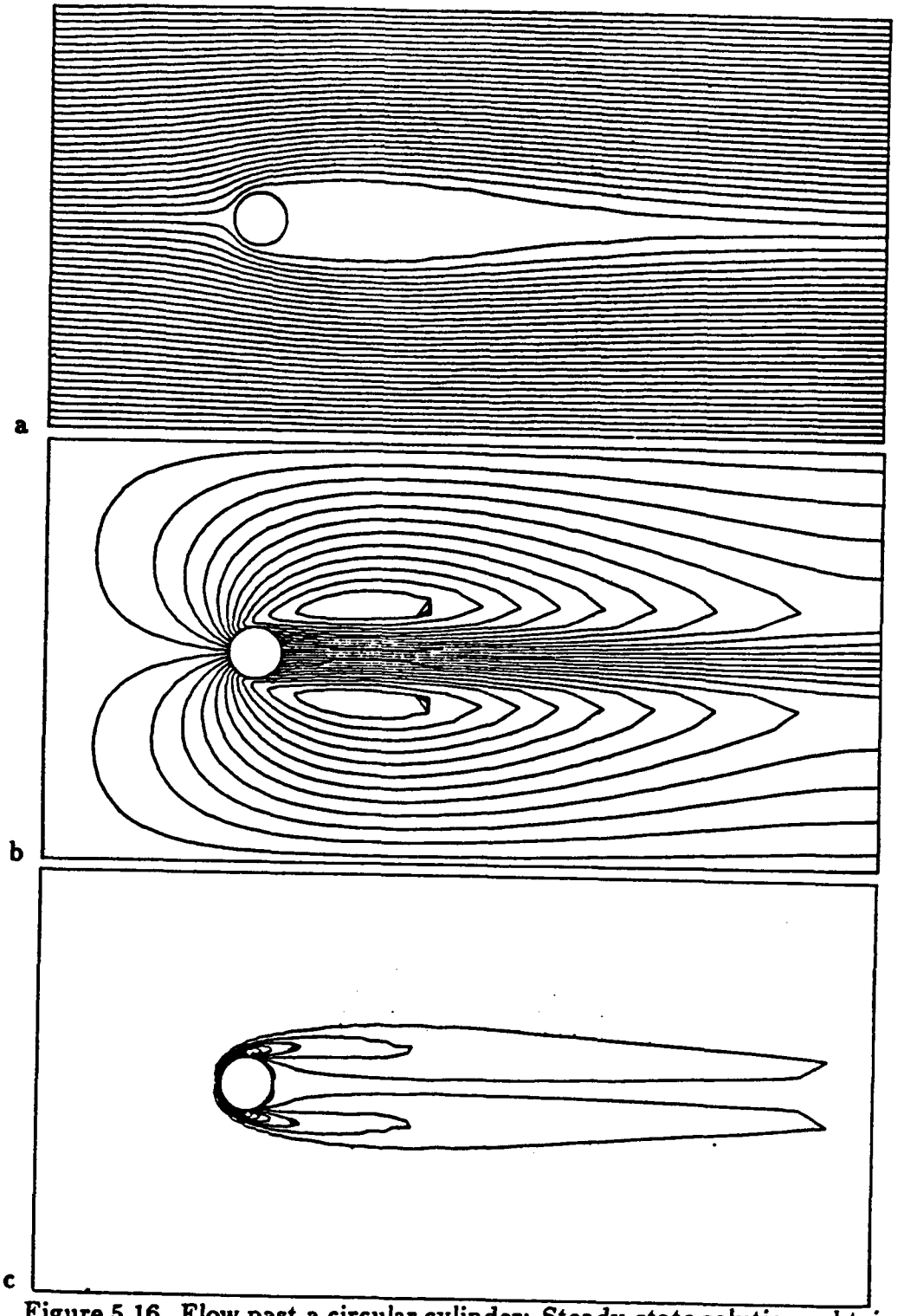

Figure 5.16. Flow past a circular cylinder: Steady-state solutions obtained by the vorticity stream-function formulation at Re=100; a) Streamlines; b) Stationary streamlines; c) Vorticity.

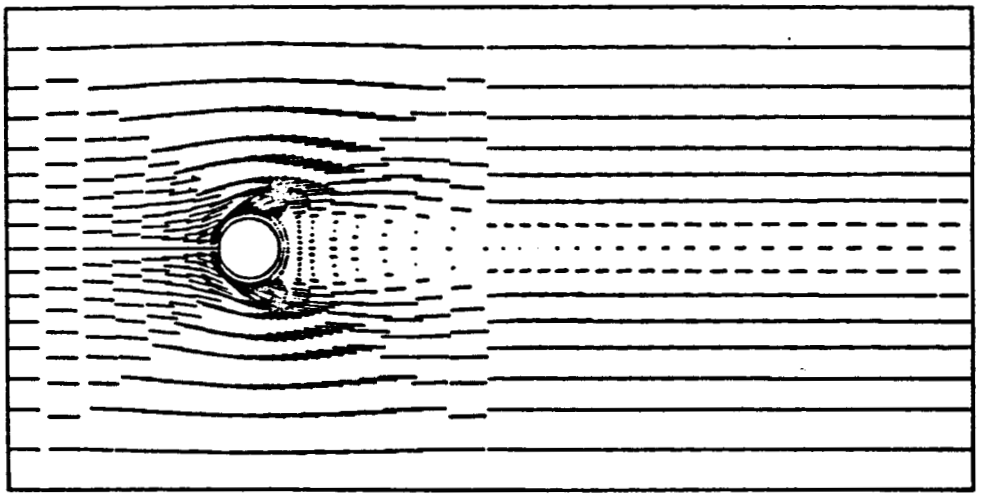

a

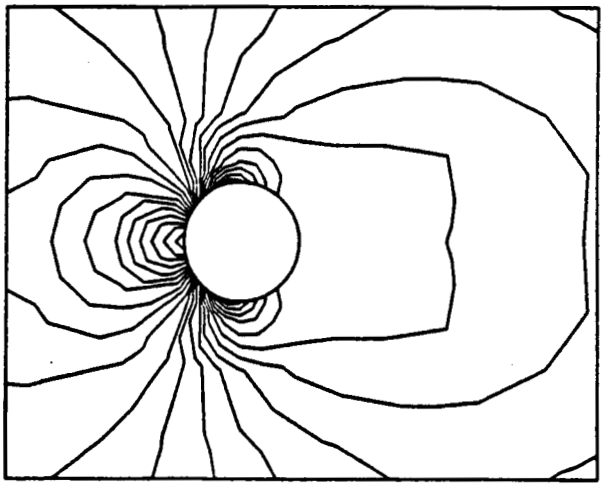

b

Figure 5.17. Flow past a circular cylinder: Steady-state solutions obtained by the velocity-pressure formulation; a) Velocity; b) Pressure.

In both situations the perturbation produces a nonsymmetrical flow field. The symmetry of the standing vortices is broken. They start oscillating and finally shed (Figures 5.18 to 5.23).

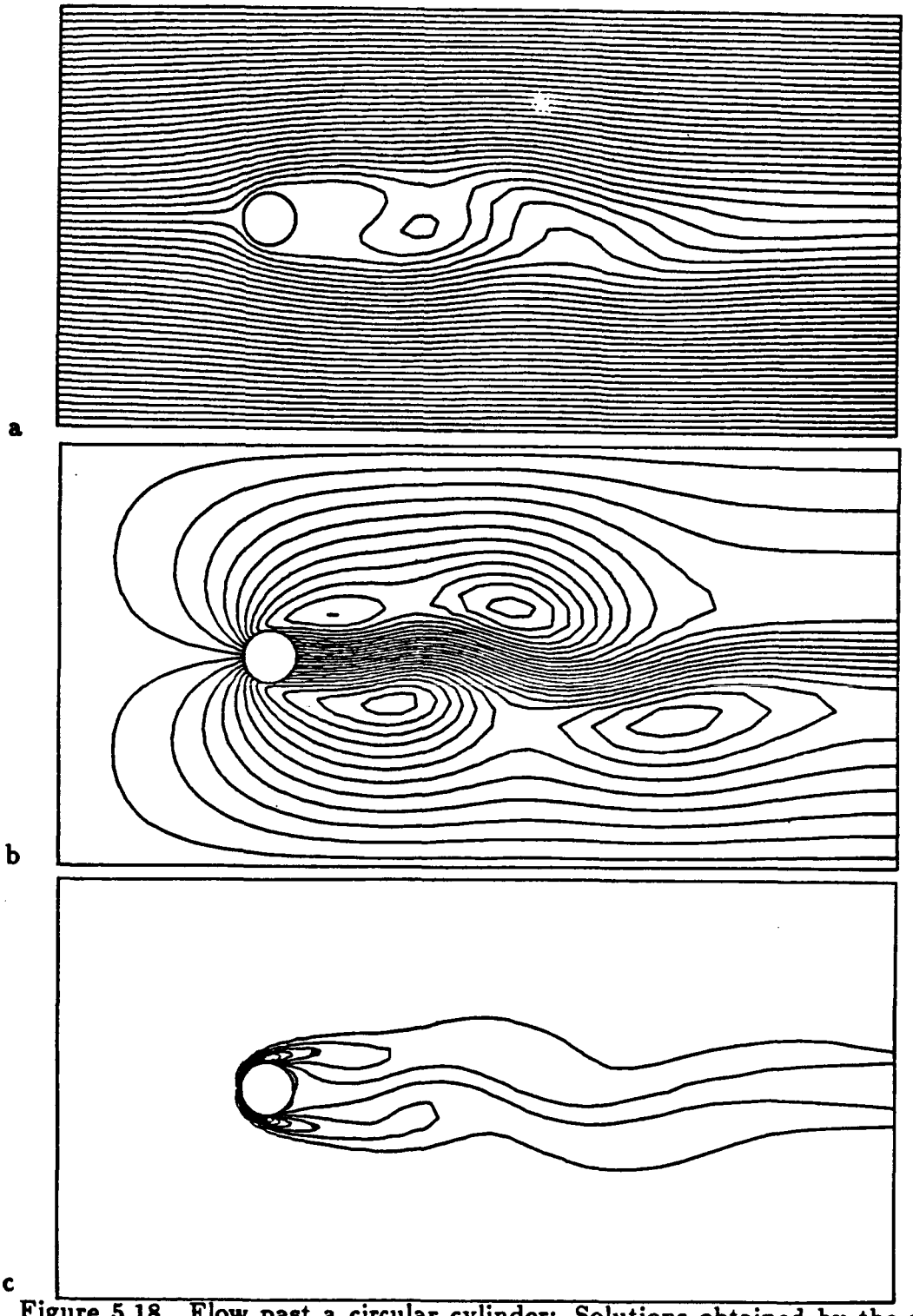

Figure 5.18. Flow past a circular cylinder: Solutions obtained by the vorticity stream-function formulation at Re=100 at t=120s after perturbation; a) Streamlines; b) Stationary streamlines; c) Vorticity.

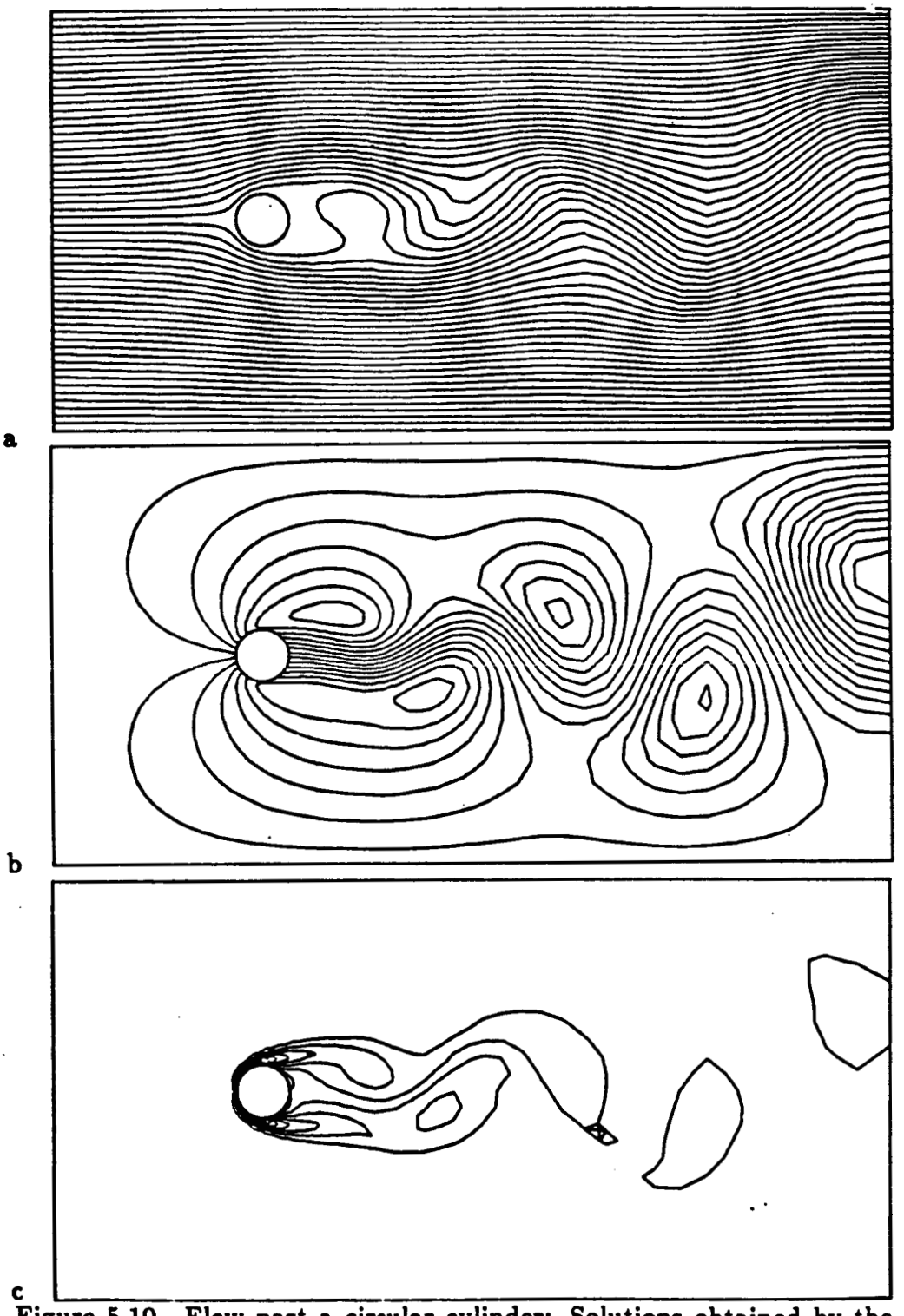

Figure 5.19. Flow past a circular cylinder: Solutions obtained by the vorticity stream-function formulation at Re=100 at t=240s after perturbation; a) Streamlines; b) Stationary streamlines; c) Vorticity.

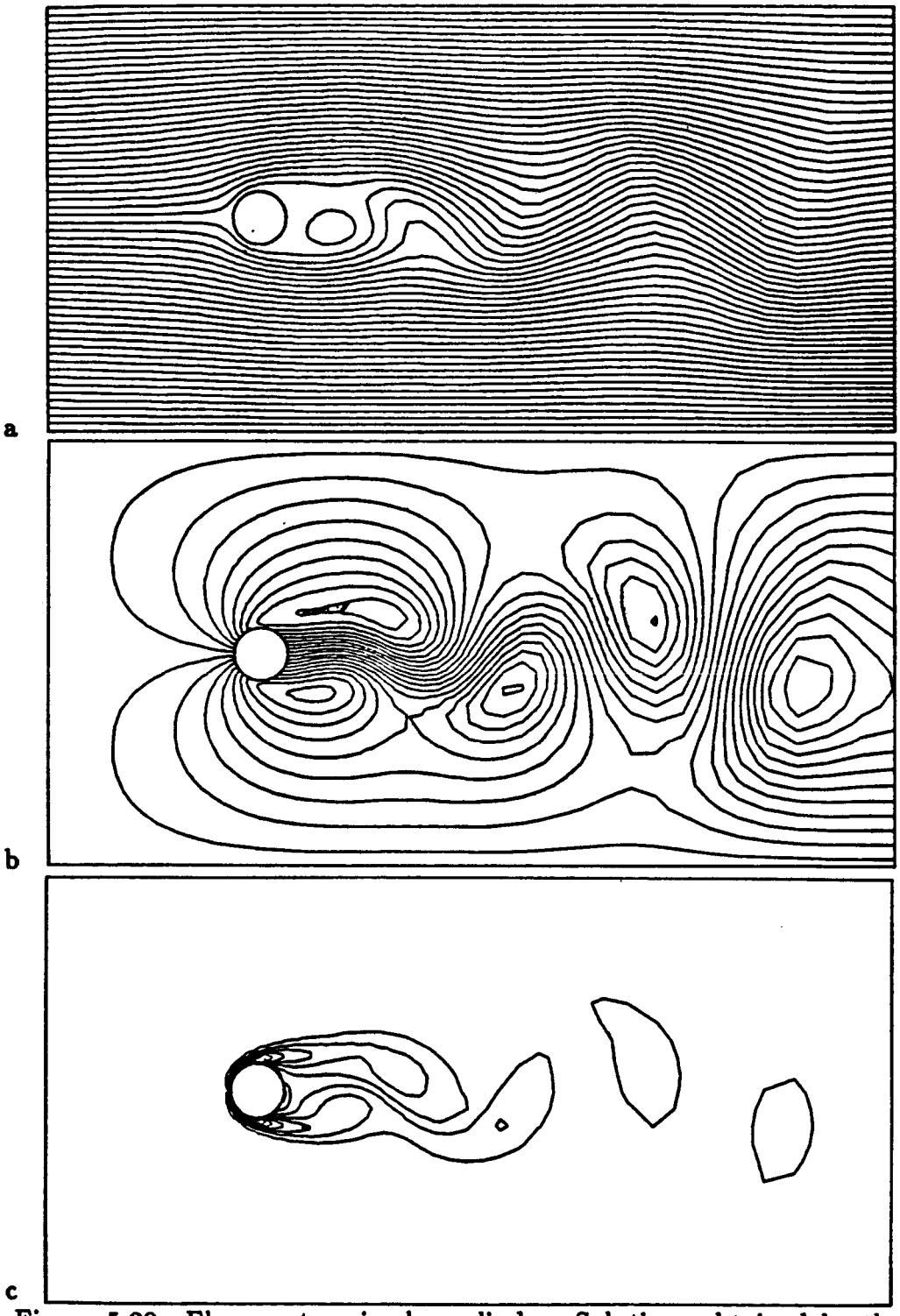

Figure 5.20. Flow past a circular cylinder: Solutions obtained by the vorticity stream-function formulation at Re=100 at t=360s after perturbation; a) Streamlines; b) Stationary streamlines; c) Vorticity.

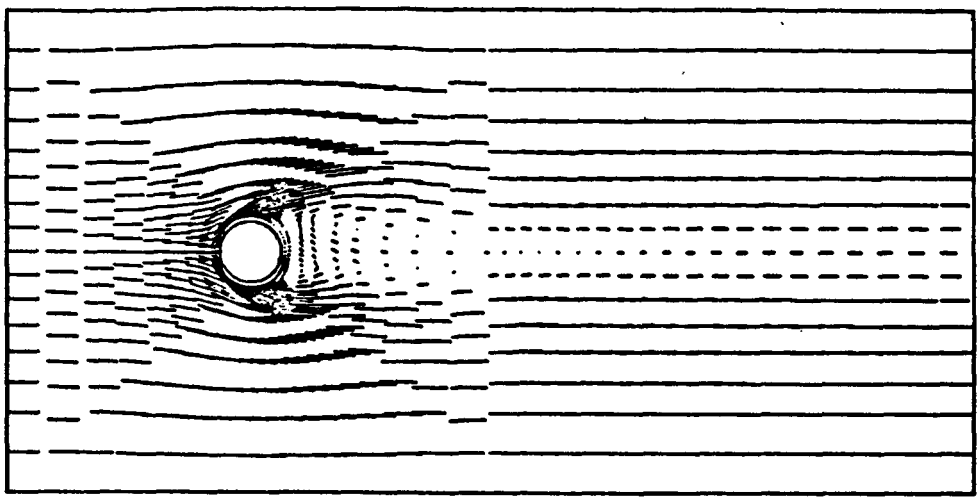

a

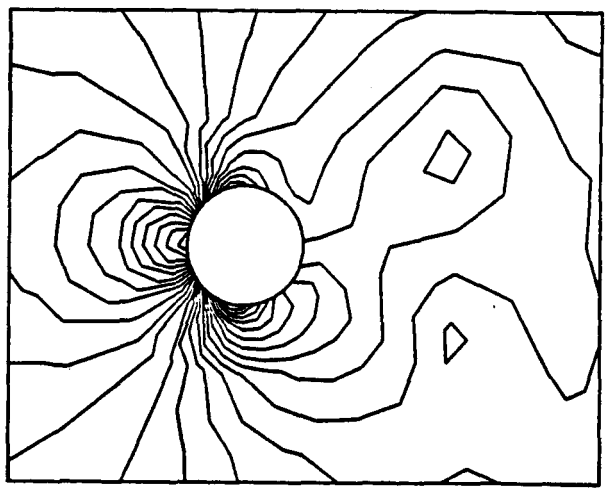

b

Figure 5.21. Flow past a circular cylinder: Solutions obtained by the velocity-pressure formulation at Re=100 at t=15s after perturbation; a) Velocity; b) Pressure.

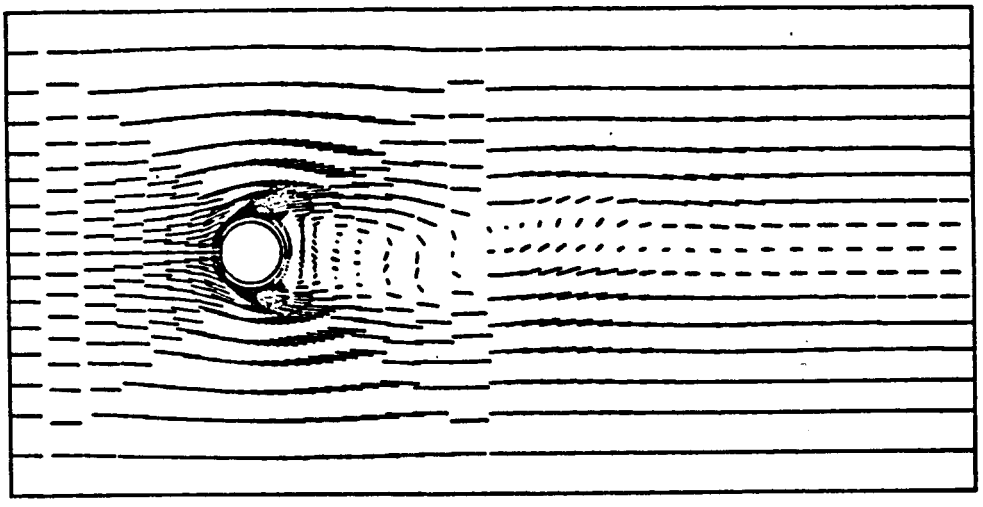

a

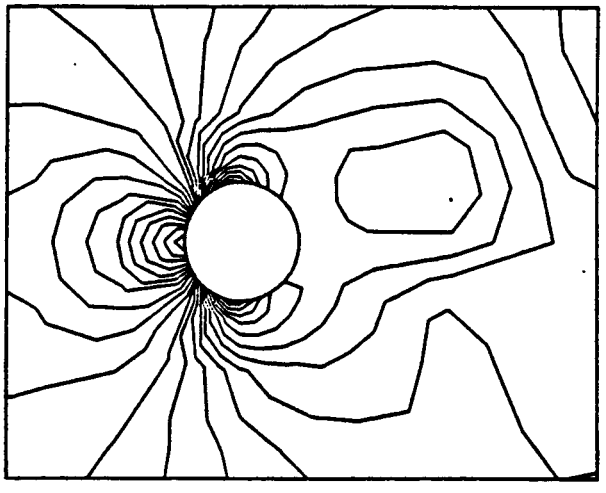

b

Figure 5.22. Flow past a circular cylinder: Solutions obtained by the velocity-pressure formulation at Re=100 at t=105s after perturbation; a) Velocity; b) Pressure.

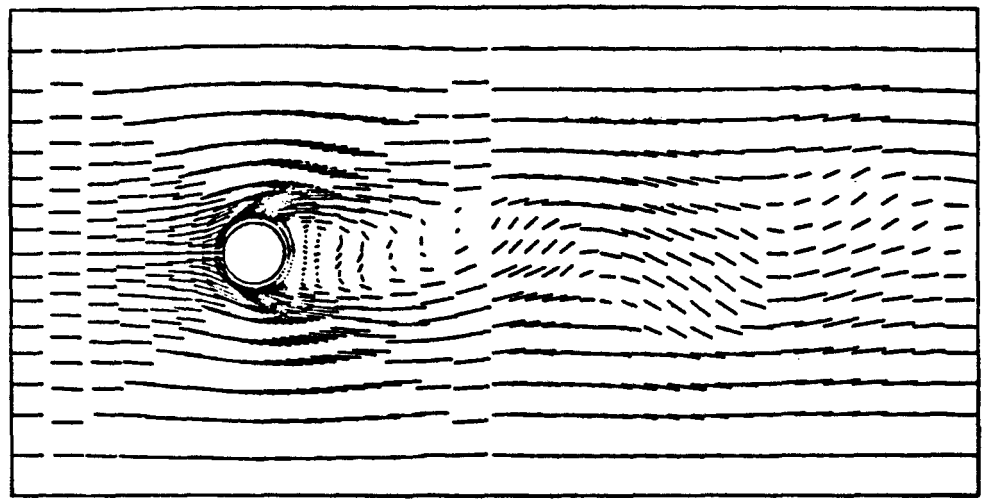

a

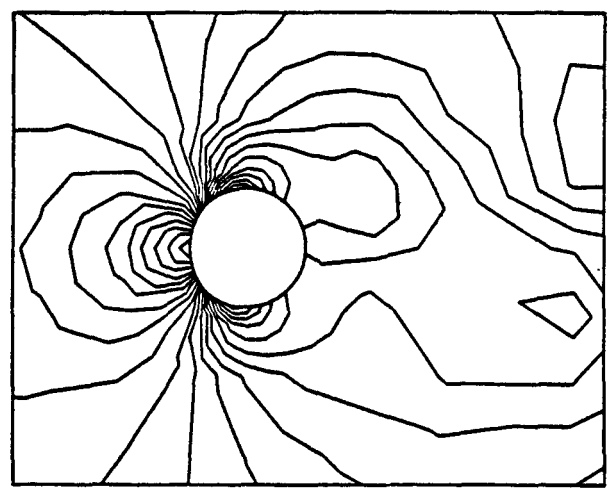

b

Figure 5.23. Flow past a circular cylinder: Solutions obtained by the velocity-pressure formulation at Re=100 at t=180s after perturbation; a) Velocity; b) Pressure.

CHAPTER 6: CONCLUSIONS

The present study has focused on the development of streamline-upwind/ Petrov-Galerkin finite-element procedures for the Navier-Stokes equations in both the primitive variable and the vorticity stream-function formulations. The abilities of the two methods for simulating internal and external flows have been studied. For all test cases the results are in good agreement with available data.

The main advantages of the vorticity stream-function formulation are the simple form of the equations in two-dimensions and the in-built satisfaction of the incompressibility constraint.

In two dimensions, the vorticity transport equation and the Poisson equation for the stream function are scalar and there are only two degree of freedom in the problem. Moreover, the vorticity stream-function form of the Navier-Stokes equations allows equal order of interpolation for the vorticity and the stream function. In fact the bilinear interpolations which have been used here for both the unknowns are sufficient which is an asset from the point of view of implementation.

On the other hand, a flow field obtained by the solution of the vorticity stream-function equations is by definition divergence-free and the initial condition of the problem do not need to satisfy the incompressibility constraint. This allows the use of an initial flow field noncontinuous at the boundary of the domain.

In the case of the primitive variable formulation in two dimensions, the number of degrees of freedom is three. Moreover in this formulation the use of equal orders of interpolation for pressure and velocity can lead to erroneous pressure solutions such as checkerboard modes. Mixed interpolations are usually used in which implementation is less straightforward than equal order of interpolation. Here we implemented a mixed interpolation using the nine-node Lagrange element and a four-node + bubble element. The latter exhibits a checkerboad mode which can be treated through smoothing techniques. On the other hand, in the velocity-pressure method, the pressure is adjusted to satisfy the incompressibility constraint in a weak sense.

From the point of view of the boundary conditions, the velocity-pressure formulation allows a more natural implementation than the vorticity stream-function formulation especially for flow domains having inner boudaries. In that case,the vorticity stream-function formulation provides only approximate boundary conditions for the stream function and no conditions for vorticity. In the present study, the simulation of the flow around a cylinder is possible under the assumption of symmetry of the flow pattern at the upstream of the cylinder. When the flow is perturbed, this assumption is not valid, but in the present scheme, the stream function cannot be updated at the inner boundary. The case of a flow with multiple inner boundaries, such as an array of cylinder, cannot be handled by this scheme.

The velocity-pressure formulation allows a good treatment of the boundary

conditions. The no-slip and no-penetration conditions at solid surfaces are easy to implement. Moreover there would be no problem for handling flows in domains with multiple solid boundaries.

At a last point, the extension of the codes to three dimensions is not easy for the vorticity stream-function formulation. In three dimensions, the vorticity-stretching term does not vanish and the equation system has two nonlinear terms.

The primitive formulation can be extended to three dimensions without major difficulties. In the present study, the use of an explicit time-integration scheme obtained via a mass-lumping technique reduces the storage requirements of the scheme, and would be a significant asset for the solution of three-dimensional problems.

The possibilities for improvements and further developments of the present work are manifold.

In the case of the vorticity stream-function formulation the main improvement that can be made is a better treatment of the boundary conditions for the vorticity and the stream function at solid surfaces. In particular the need for a scheme allowing the treatment of flows in domains with multiple solid boundaries is obvious. This has been implemented by Liou [24] following the scheme proposed in [1].

Two major directions of development are possible for the velocity-pressure formulation.

The first possibility is to add the temperature as a physical unknowns in the problem. This can be obtained by coupling the energy equation to the momentum equation and the incompressibility constraint. Based on the present formulation, Ganjoo [25] has implemented that problem and obtained results comparing well with those presented in [5].

The second major development to the present work is the extension to three dimensions. As described earlier, the velocity-pressure formulation has been implemented in order that this extension be possible without dramatic changes in the algorithm. The trend in CFD is to go to three-dimensional simulations, and the present formulation is a good basis for such development.

REFERENCES

1. BRISTEAU M.O., R. GLOWINSKI and J. PERIAUX - Numerical methods for the Navier-Stokes equations ; Applications to the simulation of compressible and incompressible viscous flows, to appear in Computer Physics Report.

2. PEETERS M.F., W.G. HABASHI and E.G. DUECK - Finite element stream function - vorticity solutions of the incompressible Navier-Stokes equations, International Journal for Numerical Methods in Fluids, Vol.7, pp. 17-27 ,1987.

3. GRESHO P.M., S.T. CHAN, R.L. LEE and C.D. UPSON - A modified finite element method for solving the time-dependent, incompressible Navier-Stokes equations. Part 1: Theory, International Journal for Numerical Methods in Fluids, Vol. 4, pp. 557-598, 1984.

4. GRESHO P.M., S.T. CHAN, R.L. LEE and C.D. UPSON - A modified finite element method for solving the time-dependent, incompressible Navier-Stokes equations. Part 2: Applications, International Journal for Numerical Methods in Fluids, Vol. 4, pp. 619-640, 1984.

5. GRESHO P.M., R.L. LEE, S.T. CHAN and R.L. SANI - Solution of the time-dependent Navier-Stokes and Boussinesq equations using the Galerkin finite-element method, Lecture Notes in Mathematics, Vol. 771, pp. 203-222, 1979.

6. SANI R.L., P.M. GRESHO, R.L. LEE - On the spurious pressures generated by certain GFEM solutions of the incompressible Navier-Stokes equations, Proceedings of the Third International Conference on Finite Elements in Flow Problems, Banff, Canada, 1980.

7. HUGHES T.J.R. and A.N. BROOKS - A theoretical framework for Petrov-Galerkin methods with discontinuous weighting functions: Application to the streamline-upwind procedure, R.H Gallagher, eds. D.N. Norrie, J.T. Oden and O.C. Zienkiewicz, Finite Elements in Fluids, pp. 46-65 ,Wiley, London, 1982.

8. BROOKS A.N. and T.J.R. HUGHES - Streamline-upwind/Petrov-Galerkin formulations for convection-dominated flows with particular emphasis on the incompressible Navier-Stokes equations, Computer Methods in Applied Mechanics and Engineering, Vol. 32, pp. 199 - 259 , 1982.

9. TEZDUYAR T.E. and T.J.R. HUGHES - Finite-element formulations for convection-dominated flows with particular emphasis on the compressible Euler equations, Proceedings AIAA 21st Aerospace Sciences Meeting, AIAA Paper 83-0125, Reno, NV,1983.

10. HUGHES T.J.R., M. MALLET and L.P. FRANCA - Entropy-stable finite element methods for compressible fluids: Application for high Mach number flows with shocks, in : Finite Element Methods for Nonlinear Problems, Springer, Berlin,1986.

11. TEZDUYAR, T.E and D.K. GANJOO - Petrov-Galerkin formulations with weighting functions dependent upon spatial and temporal discretizations : applications to transient convection-diffusion problems, Computer Methods in Applied Mechanics and Engineering, Vol. 59, pp. 49 - 71, 1986

12. TEZDUYAR T.E. and Y.J. PARK - Discontinuity-capturing finite-element formulations for nonlinear convection-diffusion-reaction equations, Computer Methods in Applied Mechanics and Engineering, Vol. 59, pp. 307-325, 1986.

13. POTTER M.C and J.F FOSS - Fluid Mechanics, Ronald Press, New York, 1975.

14. TEZDUYAR T.E., R. GLOWINSKI, F. GLAISNER - Streamline-upwind/ Petrov-Galerkin procedures for the vorticity stream-function form of the Navier-Stokes equations, to be presented at the Fifth International Conference on Numerical Methods for Laminar and Turbulent Flows, Montreal, July 1987.

15. DONEA J., T. BELYTSCHKO and P. SMOLINSKI - A generalized Galerkin method for steady convection-diffusion problems with application to quadratic shape function elements, Computer Methods in Applied Mechanics and Engineering, Vol. 32, pp. 25-43, 1985

16. ROACHE P.J. - Computational fluid dynamics, Hermosa Publishers, 1972.

17. HUYAKORN P.S., C. TAYLOR, R.L. LEE and P.M. GRESHO - A comparison of various mixed-interpolation finite elements in the velocity-pressure formulation of the Navier-Stokes equations, Computers and Fluids, Vol. 6, pp. 25-35, 1978.

18. LEE R.L., P.M. GRESHO and R.L. SANI - Smoothing techniques for certain primitive variable solutions of the Navier-Stokes equations, International Journal for Numerical Methods in Engineering, Vol. 14, pp. 1785-1804, 1979.

19. HUGHES T.J.R., W.K. LIU, A. BROOKS - Finite element analysis of incompressible viscous flow by the penalty function formulation, Journal of Computational Physics, Vol. 39, pp. 1-60, 1979.

20. SCHREIBER R. and H.B. KELLER - Driven cavity flows by efficient numerical techniques, Journal of Computational Physics, Vol. 49, pp. 310-333, 1983.

21. BRAZA M., P. CHASSAING and H. HA MINH - Numerical study and physical analysis of the pressure and velocity fields in the near wake of a circular cylinder, Journal of Fluid Mechanics, Vol. 165, pp. 79-130, 1986.

22. FORNBERG B. - A numerical study of steady viscous flow past a circular cylinder, Journal of Fluid Mechanics, Vol. 98, pp. 819-855, 1980.

23. TANEDA S. - Experimental investigation of the wakes behind cylinders and plates at low Reynolds numbers, Journal of the Physical Society of Japan, Vol. 11, 3, pp.302-307, 1956.

24. LIOU J. - Private communication, 1987.

25. GANJOO D.K. - Private communication, 1987.